6-1-2011

Dynamic contrast-Enhanced MRI of Pancreatic Islet Transplants

Nathaniel K. Chan
Loma Linda University

LOMA LINDA UNIVERSITY
School of Medicine
in conjunction with the
Faculty of Graduate Studies

Dynamic Contrast-Enhanced MRI of Pancreatic Islet Transplants

by

Nathaniel K. Chan

A Dissertation submitted in partial satisfaction of
the requirements for the degree of
Doctor of Philosophy in Biochemistry

June 2011

Each person whose signature appears below certifies that this dissertation in his/her opinion is adequate, in scope and quality, as a dissertation for the degree Doctor of Philosophy.

_____, Chairperson
Eba Hathout, Professor of Pediatrics

_____
Penelope Duerksen-Hughes, Associate Dean for Basic Sciences and Translational Research and Professor of Basic Sciences

_____
Wolff Kirsch, Professor of Basic Sciences and Neurosurgery

_____
Andre Obenaus, Associate Professor of Biophysics and Bioengineering, Pediatrics, Radiation Medicine, and Radiology

_____
Lawrence Sowers, Professor of Biochemistry

ACKNOWLEDGEMENTS

> "In attestation of his wondrous wisdom, both the Heavens and the Earth present us with innumerable proofs not only those more recondite proofs which astronomy, medicine, and all the natural sciences, are designed to illustrate, but proofs which force themselves on the notice of the most illiterate peasant, who cannot open his eyes without beholding them. It is true, indeed, that those who are more or less intimately acquainted with those liberal studies are thereby assisted and enabled to obtain a deeper insight into the secret workings of divine wisdom." - John Calvin

I would like to express my deep gratitude to Dr. Hathout, who welcomed me to her lab and has been inspirational as a mentor in her deft balancing of clinical responsibilities, research duties, and family life. I am indebted to Dr. Sowers for not only introducing me to Dr. Hathout, but his long-standing support of my work. I am grateful to my committee for their careful reading and guidance in dissertation preparation.

Finally I thank my family for being a respite from the rigors of research. Isaac Newton famously wrote in 1676, "If I have seen further it is only by standing on the shoulders of giants." I must acknowledge that I have come this far in my studies only by being supported high on the shoulders of my mother. Though she may be of petite physical stature, her sacrifices and unceasing care and love are immense. This work is dedicated to her.

CONTENTS

FIGURES

Figure Page

ABBREVIATIONS

DCE MRI	Dynamic Contrast-Enhanced Magnetic Resonance Imaging
T1DM	Type 1 Diabetes Mellitus
POD	Post-Operative Day
HBO	Hyperbaric Oxygen
STZ	Streptozotocin
K_{trans}	vessel permeability constant
AUC	Area Under the Curve
GTT	Glucose Tolerance Test
AIF	Arterial Input Function
HIF-1α	Hypoxia Inducible Factor 1, alpha
VEGF	Vascular Endothelial Growth Factor
TUNEL	Terminal deoxynucleotidyl transferase dUTP Nick End Labeling
H&E	Hematoxylin & Eosin
vWF	vonWillebrand Factor
NSF	Nephrogenic Systemic Fibrosis
MSC	Mesenchymal Stem Cell

ABSTRACT OF THE DISSERTATION

Dynamic Contrast-Enhanced MRI of Pancreatic Islet Transplants

by

Nathaniel K. Chan

Doctor of Philosophy, Graduate Program in Biochemistry
Loma Linda University, May 2011
Dr. Eba Hathout, Chairperson

Since its discovery in 1922, insulin has been the life-saving treatment for type 1 diabetes mellitus. As the disease is caused by the loss of insulin-producing pancreatic islets, transplantation of donor islets has the potential to not only supplement insulin replacement therapy but to cure type 1 diabetes. However, long-term insulin independence (> 2 years post-transplant) remains a challenge partly due to low islet blood flow immediately following transplantation leading to hypoxic stress on islets. The goal of our studies is to improve islet engraftment by monitoring and promoting the regrowth and maturation of new islet blood vessels in a clinically applicable manner. The developed technique is based on intravascular injection of a FDA-approved contrast agent which leaks from and accumulates around permeable immature blood vessels. Rapidly acquired MRI scans following contrast administration can then show the location and extent of new vessel formations. Our studies showed dynamic contrast-enhanced MRI to be successful in determining a timeline for islet revascularization as well as evaluating the effectiveness of a hyperbaric oxygen-based engraftment-enhancing therapy. The results are an important step in advancing islet transplantation as a potential cure for type 1 diabetes.

CHAPTER ONE

INTRODUCTION

Type 1 Diabetes Mellitus

Type 1 diabetes mellitus (T1DM) is characterized by the loss of insulin secreting pancreatic islets and resultant hyperglycemia. The disease is fatal unless treated with exogenous insulin, which is currently the standard of care. However, as Frederick Grant Banting, the Canadian surgeon credited with the co-discovery of insulin (Banting 1922) concluded in his Nobel lecture, "insulin is not a cure for diabetes; it is a treatment." True to this day, the lifetime costs of diabetes treatment are very high, and the global incidence of type 1 DM is rising (Aanstoot 2007).

Both genetic and environmental factors seem to play a role in the development of type 1 diabetes. It is thought that autoimmunity develops from macrophage scavenging of islet autoantigens and presentation by major histocompatibility complex (MHC) class II molecules, leading to the activation of helper T-cells, in turn activating B-cells to produce autoantibodies as well as activate killer cells and cytotoxic T-cells (Atkinson 2011). It follows that several alleles of the major histocompatibility complex, class II, DQ beta 1 (HLA-DQB1) gene have been found to be associated with an increased risk of developing type 1 diabetes (Redondo 2001). This gene codes for one of two proteins that make up the antigen-presenting cell surface receptor DQ heterodimer, and is the most predictive gene identified so far. However, less than 10% of genetically susceptible people progress to onset of disease. Combined with the finding that pairwise

concordance for T1DM is less than 40% in identical twins (Kaprio 1992), this implies that additional environmental factors can act as triggers in predisposed individuals. The initial islet inflammatory response to autoimmune attack results in subclinical insulitis, and exogenous factors seem to also play a role in determining the rate of islet mass destruction, resulting ultimately in clinical disease (Knip 2005).

As understanding of immune modulation has grown, so has the hope of being able to interrupt the autoimmune process. It has become increasingly clear that the balance between regulatory and effector T-cells is a main determinant of disease risk (Bour-Jordan 2009, McClymont 2011), and that immune-modulatory therapies have the potential to be used in preventative and curative capacities (Bluestone 2010). Advances in the ability to induce tolerance are particularly relevant to the future success of transplantation based therapies (Turka 2010, Ishiyama 2011).

Islet Transplantation

Restoring islet mass in type 1 diabetic patients with donor islet transplantation is one curative strategy based on the isolation and purification of only the insulin producing islets from the rest of the exocrine pancreas. Isolated islets are then infused into the portal vein of the liver, where they lodge in the vascular bed of the liver lobes. Paul Lacy is often credited as the father of islet transplantation, as he led the research efforts at Washington University which resulted in the first successful human islet transplantation in 1989 (Scharp 1990). Use of the mechanical device known as a Ricordi chamber (Ricordi 1990) to automate part of the islet isolation procedure was instrumental in recovering a sufficiently large islet mass for achieving insulin independence (Tzakis

1990). Despite these early efforts, consistent and sustained (>1 year) insulin independence was not achieved until recently in a small cohort of seven patients in Edmonton, Canada (Shapiro 2000). Disappointingly, a subsequent multi-center international trial of the Edmonton protocol showed that the majority of islet recipients needed to resume the administration of insulin two years post-transplantation (Ryan 2005).

Native islets are highly vascularized structures that make up only a few percent of pancreatic tissue by mass, but receive about ten percent of pancreatic blood flow in keeping with their endocrine function. Only recently has the dense vascular network of a pancreatic islet been directly, albeit invasively, visualized *in vivo* by real-time laser confocal microscopy (Nyman 2008). Upon isolation, donor islets are removed from this rich vascular network. This islet avascularity in the early post-transplant period poses a serious hypoxic threat (Miao 2006) and leads to a significant loss of transplanted islets.

Magnetic Resonance Imaging

To address this islet hypoxia, our goal is to improve islet engraftment by monitoring and promoting islet angiogenesis with an eye toward clinical applicability, which calls for non-invasive methods. One way of non-invasively measuring *in vivo* vascularity and blood flow is with dynamic contrast-enhanced magnetic resonance imaging (DCE MRI). Pioneering work on this imaging modality was done for the study of blood vessels in tumors (Knopp 2001, Padhani 2001, Yankeelov 2009). The operating principle is based on the intravascular injection of a bright contrast agent which subsequently leaks from and accumulates around permeable immature or damaged blood

vessels (Jordan 2005). The process and time course of contrast agent extravasation can then be imaged and quantified (Paldino 2009). The spatial resolution and specificity of the technique are appealing in its potential application to measuring angiogenesis of transplanted islets.

Specific Aims

The objectives of the following studies are to first establish a methodology to non-invasively monitor islet graft angiogenesis with dynamic contrast-enhanced MRI, and then use the technique to evaluate the effectiveness of a pro-angiogenic strategy.

Specific Aim 1

The first aim is to monitor the angiogenesis of kidney subcapsular islet grafts using DCE MRI. The feasibility of DCE MRI to detect angiogenesis will be established in a non-diabetic subcapsular islet transplant model. The subcapsular model is well established in animal studies, and the timeline of islet engraftment is well described. In addition, the localized islet graft cluster is most amenable to the established method of visualizing and analyzing DCE MRI data on tumors. Following serial non-invasive imaging, islet grafts will be recovered and assessed histologically for new microvessel growth.

Specific Aim 2

The second aim is to monitor the angiogenesis of intraportal islet grafts in the liver using DCE MRI. The DCE MRI method will be optimized to allow for imaging and analysis of intraportal islet grafts which are distributed throughout the liver lobes and undergo

respiratory motion. Imaging results will be correlated with new vessel formation seen histologically.

Specific Aim 3

The third aim is to evaluate the effectiveness of a pro-angiogenic strategy following islet transplantation. Islet hypoxia in the immediate post-transplant period negatively affects survival and islet graft mass. Hyperbaric oxygen (HBO) therapy will be tested as a treatment to reduce this local hypoxia and improve engraftment. DCE MRI of treated islet grafts will be performed and imaging data will be correlated with histological and functional metabolic studies.

CHAPTER TWO

IN VIVO IMAGING DEMONSTRATES A TIME-LINE FOR NEW VESSEL FORMATION IN ISLET TRANSPLANTATION

Eba Hathout*, Nathaniel K. Chan, Annie Tan, Naoaki Sakata, John Mace, William Pearce, Ricardo Peverini, Richard Chinnock, Lawrence Sowers and Andre Obenaus

Islet Transplant Laboratory, Department of Pediatrics, Radiation Medicine and Radiology, Loma Linda University, Loma Linda, CA, USA

Running Title: In vivo imaging of new vessel formation in islet grafts

Key words: islet transplantation, imaging, vascularization, in vivo, MRI

Abbreviations: AIF, arterial input function; AUC, area under the curve; DCE, dynamic contrast-enhanced; DTPA, diethylene triamine pentaacetic acid; FOV, field of view; H&E, hematoxylin and eosin; MR, magnetic resonance; MRI, magnetic resonance imaging; PB, Prussian Blue; SPIO, superparamagnetic iron particles; TE, echo time; TR, repetition time; vWF, von Willebrand factor.

*Eba Hathout, MD, FAAP
Professor and Chief, Division of Pediatric Endocrinology and Diabetes
Loma Linda University School of Medicine
11175 Campus Street CP A1120R
Loma Linda, CA 92354, USA
Tel.: +909 558 4773
Fax: +909 558 0408
E-mail: EHathout@llu.edu

Pediatric Transplantion. 2009 Nov;13(7):892-7

Abstract

Vascularization of transplanted islets must be maintained to provide long-term graft function. *In vivo* assessment of new vessel formation in islet grafts has been poorly documented. The purpose of this study was to investigate whether neovascularization was detectable *in vivo* in a Feridex-labeled murine syngeneic subcapsular islet mass using DCE MRI over 180 days. Subcapsular transplants could be visualized at post-transplant days three, seven, 14, and 28 using T2-weighted MRI and at post-transplant day 180 by immunohistochemistry. Injection of the contrast agent gadolinium (Gd)-DTPA for DCE at three, seven, and 14 days showed increased signal in the transplant area consistent with new vessel formation. Areas under contrast enhancement curves suggested peak angiogenesis at 14 days. At 180 days, there was no observable change in signal intensity after contrast injection suggesting established vascularization or islet mass reduction. Immunohistochemistry confirmed MRI and DCE findings. These data suggest that islet angiogenesis occurs early after transplantation and is likely established after one month of transplantation. This study provides an *in vivo* time-line of neovascularization in subcapsular islet grafts. We anticipate that contrast extravasation captured by MRI may provide useful monitoring of graft angiogenesis if reproduced in a clinically relevant intraportal model.

Introduction

Pancreatic islet transplantation is a promising therapy for patients with type 1 diabetes (1, 2). However, long-term insulin independence is frequently not sustainable presumably because of hypoxic, inflammatory, and immune damage to islets (3). In a healthy pancreas, islets are in a nutrient-rich environment with highly oxygenated blood. After transplantation, islets are subject to hypoxia from initial avascularity (4, 5), and it is estimated that approximately 50–70% of islets are lost in the immediate post-transplantation period (50–70%), along with functional impairment of the remaining surviving islets (3, 6, 7). A total of two to four pancreatic donors are sometimes required for a sufficiently functional islet transplant (1). Despite the above challenges, there is an obvious paucity of *in vivo* methods to monitor islet fate and in particular, new vessel formation in islet grafts.

Several studies have shown that *in vivo* MRI of transplanted rodents can be used to localize islets labeled with SPIO under high resolution (8–10). It has also been recently demonstrated that MRI monitoring of SPIO-labeled islets can be applied clinically to intrahepatic islet transplantation in patients with type 1 diabetes (11).

To chronicle islet graft neovascularization *in vivo*, we used contrast extravasation to characterize neovascularization. DCE MRI is an imaging modality that can be used to noninvasively measure key hemodynamic parameters such as blood flow, blood volume, interstitial volume and capillary permeability in real time. This method has been used clinically to assess tumor angiogenesis and the vascular effects of anticancer therapies (12–16).

In a pilot short-term trial, we previously reported that DCE MRI can be used to evaluate neovascularization non-invasively in islets transplanted under the kidney capsule (10). We first described a macroscopic timeline for islet angiogenesis, then confirmed that iron labeling of islets allowed localization of islet grafts as hypointense regions on post-transplant days three and 14. In our previous study, DCE MRI revealed increased contrast enhancement on day 14 compared with day three suggesting temporal evolution of new vessel formation. Here, we detail the chronology of progression of vascularization hemodynamically by including earlier and later time points, and quantify the extent of MR-captured neovascularization to allow future functional correlation studies. In addition, we present concomitant immunohistochemical identification of iron-labeled cells, islets, and new vessels.

Materials and Methods

Animals

Adult female Balb/c mice weighing 25–30 g were purchased (Charles River, Wilmington, MA, USA) and housed under specific pathogen-free conditions with a 12-h light/dark cycle and had free access to food and water. All care and handling of animals was in accordance with institutional regulations. The Loma Linda University Institutional Animal Care Use Committee approved all experimental protocols.

Islet Transplantation Studies

Islets were isolated by collagenase digestion of the pancreas and separated from exocrine tissue by a discontinuous Ficoll density gradient centrifugation and then hand-

picked (10). Iron labeling of islets was performed by overnight co-culture of freshly isolated islets in Feridex (Advanced Magnetics Inc., Cambridge, MA, USA) supplemented medium at 200 μg iron/mL as previously described (10). Five hundred syngeneic islets were transplanted under the kidney capsule of normal recipients as a single mass. Three animals were used to produce results at each time point.

MRI

MRI was performed at three, seven, 14, 28, and 180 days after transplantation. Imaging was undertaken to (i) identify the location of the islets on the kidney and (ii) use DCE imaging as a surrogate marker for angiogenesis. All MRI data were collected on a Bruker Advance 11.7TMRI (8.9 cm bore) with a 3.0 cm (ID) volume radiofrequency coil (Bruker Biospin, Billerica, MA, USA). Mice were lightly anesthetized using isoflurane (3% induction and 1% maintenance). A tail vein catheter was inserted and fastened to the tail for infusion of gadolinium-DTPA [Gd-DTPA,-BMA, Gadodiamide, 0.1 mmol/kg body weight (0.2 mL/kg), Omniscan; Amersham Health, Princeton, NJ, USA] contrast. Body temperature was maintained at 35–37 ± 1 °C using a thermostat-controlled heated water cushion placed under the mouse. Respiration was monitored with a MR-compatible pressure transducer on a Biopac MP150 (Goleta, CA, USA) system. Scout images were obtained in the axial, sagittal, and coronal planes to accurately position slices.

Three MR sequences were acquired: (i) A 10 echo T2 sequence composed of a TR/TE of 4697/10.2 ms, a 256 matrix, a 3 cm FOV, two averages for a total acquisition time of 40 min, (ii) The pre/post-contrast T1 was composed of a TR/TE of 837.1/10.2 ms, a 256 matrix, 3 cm FOV, and four averages for a total acquisition time of 14 min. The

standard T2 and T1 sequences collected 20 coronal slices that were 0.80 mm thick and interleaved by 0.80 mm, and (iii) the DCE sequence acquired one image slice through the kidney at the level of the islets using a TR/TE = 250/20 ms, 128 matrix, 3 cm FOV, one average for an acquisition time of 32 s/image and a total acquisition time of 32 min with 60 images collected.

The T2 and precontrast T1 images were visually evaluated to identify the location of the transplanted islets in each animal. The single DCE acquisition slice was then placed over the region of maximal volume of the transplanted islets. At each time point, three non-diabetic transplant recipients underwent DCE MRI to non-invasively quantify islet graft vascularization as evidenced by contrast enhancement. Contrast (Gd-DTPA 0.1 mmol/kg) was delivered as a bolus injection via tail vein catheter two min after the start of the imaging sequence.

DCE Analysis

Temporal change of signal intensity was visualized and quantified using JIM software (Thorpe Waterville, UK). Three regions of interest, islet, muscle, and kidney were outlined on the DCE images based on T1 high-resolution images. Kinetic analysis used a bidirectional two-compartment model based on the equations of Tofts (17). All signal intensities were converted to [Gd] values by averaging precontrast R1 (1/T1), and assuming that

$$R1 = R1pre + \rho\,[Gd],$$

where $\rho = 1$ as we assumed that there was no difference between plasma relaxivity (relaxivity of the contrast agent in plasma) and interstitial relaxivity (relaxivity of the

contrast agent in the extra-vascular extracellular space) and R1pre is the average precontrast R1.

In the standard Tofts model, the tissue [Gd], C_t (t) is related to the plasma [Gd], C_p (t) by:

$$C_t(t) = K^{trans} \int C_p(\tau)^{(-K^{trans}(t-\tau)/v_e)} d\tau$$

where v_e is the extra-vascular extra-cellular space volume fraction. This model neglects any contribution to the signal intensity of the passing contrast in intact blood vessels within the tissue of interest. The AIF was defined from the abdominal aorta that was visible within the slice of interest. DCE MRI tissue Gd concentration curves extracted from JIM software were normalized for inter- and intra-animal comparisons.

Histology and Immunohistochemistry

After the last imaging time point, kidneys were removed and fixed in 10% formalin and embedded in paraffin. At the level of the transplanted islets, 5-lm sections were cut with serial sections processed for H&E and PB for iron particles within the transplanted islets. Briefly, sections were immersed in 10% potassium ferrocyanide (Fisher Scientific, Pittsburg, PA, USA) for five min, in PB solution containing 5% potassium ferrocyanide and 10% hydrochloric acid for 30 min and counterstained with nuclear fast red (Sigma- Aldrich, St Louis, MO, USA).

Immunohistochemistry was performed to confirm the presence of insulin in the islets and vWF for newly formed blood vessels. Specifically, sections were deparaffininized in xylene and hydrated. To restore immunoreactivity of antigens for anti-vWF, the specimens were treated with Proteinase K (Dako, Carpinteria, CA, USA)

for two min. Endogenous peroxidase activitiy was blocked by treatment of 0.1% hydrogen peroxide for 30 min. Non-specific binding was blocked by treatment with 10% goat serum for 30 min. Specimens were incubated with either: guinea pig antiinsulin antibody (1:100; Dako) or rabbit anti-vWF (1:500; Abcam, Cambridge, MA, USA) for 90 min at room temperature. Biotinylated anti-rabbit IgG antibody treatment for 30 min was followed by streptavidin-conjugated horseradish peroxidase treatment for 30 additional minutes (Vectastain Elite ABC kit; Vector Laboratories, Burlingame, CA, USA). Bound peroxidase was developed with 3–3¢-diaminobenzidine (brown; Dako) for vWF (Red; Dako) for insulin and counterstained with hematoxylin.

Statistical Analysis

Statistical evaluation of AUC from DCE curves was performed using sigmastat software (SPPS, Chicago, IL, USA) and differences among experimental groups were considered significant for $p < 0.05$. anova was performed with a Tukey post hoc test to evaluate significance at each time point. Data were expressed as the mean ± s.e.m.

Results

Islets transplanted under the kidney capsule were readily visualized in all animals in the immediate post-transplant period. The labeled islets underwent subsequent non-invasive T2-weighted imaging at three, seven, 14, and 28 days post-transplantation. Iron-labeled islets were visualized in each animal at each time point except day 180. Arrows in Fig. 1 indicate hypointense regions under the kidney capsule characteristic of iron-labeled

islets. By 180 days post-transplantation, no labeled islets could be seen by *in vivo* MRI in any of the animals.

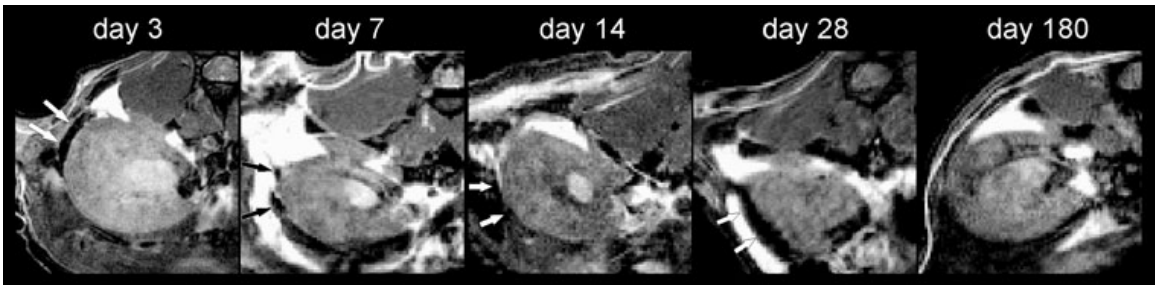

Figure 2.1. Representative T2-weighted imaging of Feridex labeled islets under the kidney capsule at three, seven, 14, 28, and 180 days post-transplantation. Islets are visible as hypointensities (white arrow) at all early time points, but not at day 180 post-transplantation.

To detect transplanted islets, histological examination was performed on days 14, 28, and 180 post-transplantation (Fig. 2). PB and insulin staining were confined to the subcapsular region of the kidney (site of the transplant). PB staining indicated the presence of iron-labeled islets at all time points. These iron-labeled islets were also seen as brown regions in the H&E sections. Insulin immunohistochemical analysis suggests a decrease in insulin staining at day 180 compared with days 14 and 28. A change in distribution of iron-positive cells is also noted over time. Iron positive cells appeared deeper within the renal parenchyma in the early time points, but were mostly in the external subcapsular margin by day 180. Staining for new vessels is shown in a separate figure.

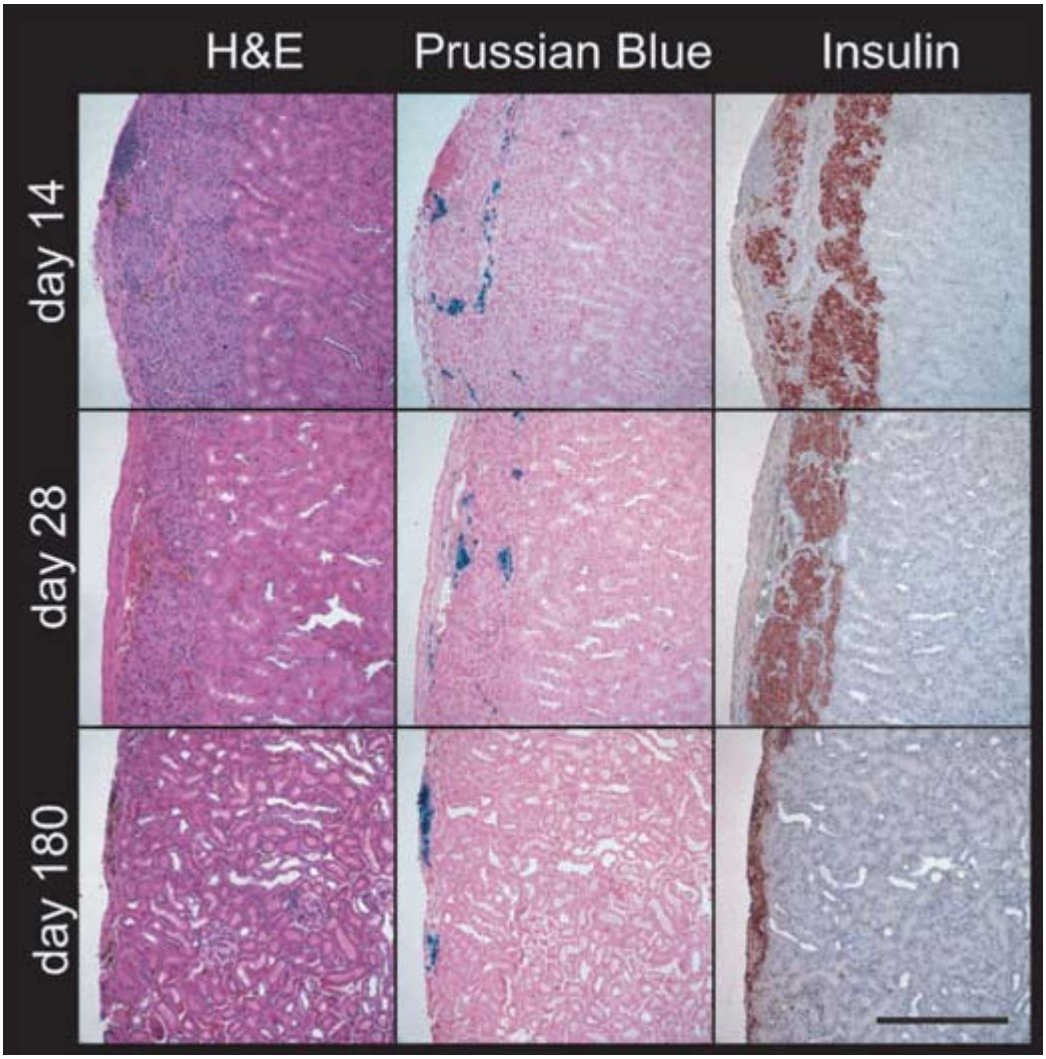

Figure 2.2. Representative immunohistochemistry of islet grafts. Kidneys with islet grafts were recovered on days 14, 28, and 180 post-transplantation, and consecutive sections were processed for H&E, PB for iron particles, and insulin for the presence of islets. PB reveals the iron-labeled islets in the subcapsular region of the kidney at days 14, 28, and 180. Unstained iron can be seen in H&E sections as brown regions at all three time points. Strong insulin immunostaining (red) shows the presence of islets at days 14 and 28 compared with weaker staining at day 180. Scale bar, 250 μm.

The dynamics of contrast enhancement in the islet grafts can be seen in Fig. 3. Normalized maximal tissue concentration of contrast increased progressively from three to 14 days, and then decreased at 28 days (Fig. 3a).

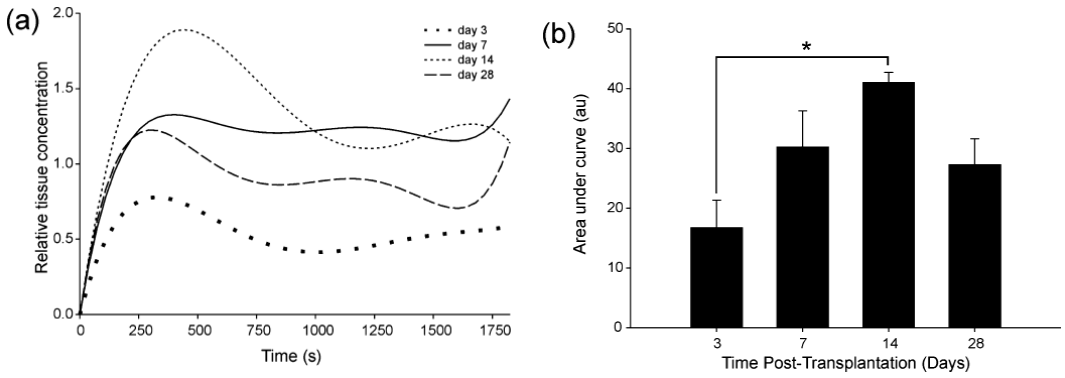

Figure 2.3. Temporal evolution of DCE MRI. (a) DCE imaging of subcapsular islet graft reveals peak enhancement at 14 days post-transplantation. (b) Area under the curve (AUC) analysis shows a progressive increase in overall enhancement over the total imaging time of 32 min (anova $p = 0.03$ with Tukey post hoc test, $p = 0.02$). Data were averaged from all animals at each time point, $n = 3$.

Time to maximal relative gadolinium concentration was 5.47 ± 1.21, 6.29 ± 2.03, 7.09 ± 0.81, and 6.26 ± 1.60 min at three, seven, 14, and 28 days, respectively. Time to peak was not significantly different between the different days, but contrast enhancement over time AUC analysis showed a clear trend towards a peak at day 14 relative to all other time points which was significant (anova $p = 0.03$, Fig. 3b). There was a significant difference in AUC between days three and 14, $p = 0.02$. AUC up to the peak concentration point showed the same trend to peak enhancement at day 14. There were no discernible islets on T2 MRI at day 180 to warrant further hemodynamic analysis.

vWF, an endothelial marker of newly formed blood vessels, was used to follow the temporal evolution of new blood vessels in the islet graft region (Fig. 4) at the same time points selected for MRI. Post-transplant day three showed disorganized vWF immunostaining, which was better outlined at day seven and more abundant at day 14.

The vWF-stained vessels at day 28 appeared larger in size, suggesting a maturation process. No vWF immunostaining was observed at day 180.

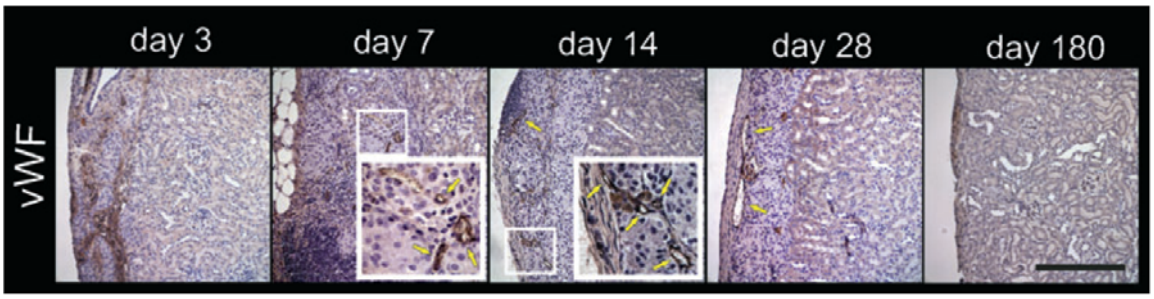

Figure 2.4. Representative temporal vascularization of islet grafts. Kidneys with islet grafts were recovered on days 3, 7, 14, 28, and 180 post-transplantation, and immunohistochemistry of anti-vWF (brown; a marker of newly formed blood vessels) was performed. Day 3 shows disorganized staining of vWF. Day 7 shows some microvessels, which are more clearly delineated at day 14 (yellow arrows indicate vessels). Day 28 is similar to day 14 with apparently larger microvessels. Day 180 shows absence of vWF staining. [These sections were immediately adjacent to sections in Fig. 2. Hence the brown in day 180 indicates iron not vWF as can be seen in corresponding H&E section (Fig. 2)]. Scale bar, 250 μm.

Discussion

In the above study, we tested the applicability of DCE MRI for assessment of neovascularization in islet grafts. To our knowledge, this is the first study to employ the clinically applicable concept of contrast extravasation to the field of islet transplantation. Lack of long-term visualization of labeled islets by MRI in our study contrasts with data by others (8, 9) who transplanted up to 1000 islets under the kidney capsule. Therefore, MR visibility may be highly dependent on islet number, and the negative localization of islets at 180 days in our study may be related to the smaller (500) islet mass we used. In addition, islet loss or redistribution over time may have lead to the reduced T2 signal and lack of visualization by MRI.

Analysis of areas under contrast enhancement curves was only significant at day 14. The trend portrayed by the curves is consistent with both our histological data, as well as reports by other groups (18–20). It is possible therefore that the use of more animals would result in significant differences at seven and 28 days. Use of heat-inactivated islets for transplantation could serve as a control for density and mass effects.

It remains to be validated whether the use of a two-compartment model is optimal for the assessment of an islet graft, or whether a three compartment model needs to be developed. As contrast enhancement is assessed relative to aortic blood flow, normalization of data may be refined by testing the variability of the AIF between study subjects. To balance sensitivity and specificity of islet imaging, positron emission tomography may be needed in addition to MRI for adequate islet volume assessment.

Our histological data show a change of distribution of iron-positive cells with time. This may reflect the lack of specificity of iron labeling or subsequent uptake of dead islets by macrophages. Such ‘‘false labeling’’ therefore can lead to overestimation of islet mass at the early post-transplant stage. Transplantation of an adequate islet mass under the kidney capsule may be visible on T2 MRI without iron labeling, a concept which would be more appealing in clinical practice. The apparent decrease in insulin-positive cells with time is consistent with previously described post-transplant islet loss, which might have been more or less exaggerated if human islets were used in an immunodeficient model.

Immunohistochemical staining results suggest that new vessel formation starts by post-transplant day three, peaks at day 14, and is complete after day 28. The use of vWF as a marker of new vessel formation has not been agreed on particularly in rodent models

where it has previously produced inconsistent results (20–22). It is also unclear whether endothelial markers for microvessels are different from macrovessels. At day 180, it is safe to assume that a mature network of blood vessels supplies the islets as they were clearly present at this late time point albeit drastically reduced in number. Thus, a marker for established rather than evolving blood vessels, e.g., alpha smooth muscle actin, might have confirmed and complemented the vascularization time-line shown above.

The small recipient numbers and lack of microvascular density quantification make this more of a pilot trial which can greatly benefit from future in depth larger scale analysis. A natural extension of this study would be to use DCE MRI in assessment of islet neovascularization in a diabetic model correlating DCE data with islet function. The ultimate *in vivo* methodology for assessment of islet neovascularization, including mathematical models, will likely be very dependent on the transplant site, and the general progress of *in vivo* imaging modalities applicable to transplanted and native islets.

The new knowledge contributed by the authors includes the non-invasive determination of a timeline of islet graft angiogenesis coupled with correlative histology. Our study offers what we believe to be a valid approach to addressing the dynamics of vascularization of islet grafts. Such hemodynamic monitoring, if applicable in an intraportal model, may be relevant to other cellular and organ transplants, and thus pave the way to strategies enhancing graft survival in clinical settings.

Acknowledgments

This work was supported by NIH/NIDDK grant number 1R01-DK077541 (EH). We are very grateful for the technical assistance provided by John Chrisler, Pete Hayes, John Hough, and Serafin Lalas.

References

1. Shapiro AM, Lakey JR, Ryan EA, et al. Islet transplantation in seven patients with type 1 diabetes mellitus using a glucocorticoid- free immunosuppressive regimen. N Engl J Med 2000: 343: 230–238.

2. Ryan EA, Paty BW, Senior PA, et al. Five-year follow-up after clinical islet transplantation. Diabetes 2005: 54: 2060–2069.

3. Davalli AM, Ogawa Y, Ricordi C, Scharp DW, Bonner -Weir S, Weir GC. A selective decrease in the beta cell mass of human islets transplanted into diabetic nude mice. Transplantation 1995: 59: 817–820.

4. Carlsson PO, Palm F, Mattsson G. Low revascularization of experimentally transplanted human pancreatic islets. J Clin Endocrinol Metab 2002: 87: 5418–5423.

5. Mattsson G, Jansson L, Carlsson PO. Decreased vascular density in mouse pancreatic islets after transplantation. Diabetes 2002: 51: 1362–1366.

6. Davalli AM, Scaglia L, Zangen DH, Hollister J, Bonner- Weir S, Weir GC. Vulnerability of islets in the immediate posttransplantation period. Dynamic changes in structure and function. Diabetes 1996: 45: 1161–1167.

7. Mattsson G, Jansson L, Nordin A, Andersson A, Carlsson PO. Evidence of functional impairment of syngeneically transplanted mouse pancreatic islets retrieved from the liver. Diabetes 2004: 53: 948–954.

8. Evgenov NV, Medarova Z, Dai G, Bonner-Weir S, Moore A. In vivo imaging of islet transplantation. Nat Med 2006: 12: 144– 148.

9. Jirak D, Kriz J, Herynek V, et al. MRI of transplanted pancreatic islets. Magn Reson Med 2004: 52: 1228–1233.

10. Hathout E, Sowers L, Wang R, et al. In vivo magnetic resonance imaging of vascularization in islet transplantation. Transpl Int 2007: 20: 1059–1065.

11. Toso C, Vallee JP, Morel P, et al. Clinical magnetic resonance imaging of pancreatic islet grafts after iron nanoparticle labeling. Am J Transplant 2008: 8: 701–706.

12. Cuenod CA, Fournier L, Balvay D, Guinebretiere JM. Tumor angiogenesis: Pathophysiology and implications for contrast-enhanced MRI and CT assessment. Abdom Imaging 2006: 31: 188–193.

13. Cartwright L, Farhat WA, Sherman C, et al. Dynamic contrast-enhanced MRI to quantify VEGF-enhanced tissueengineered bladder graft neovascularization: Pilot study. J Biomed Mater Res A 2006: 77: 390–395.

14. Medved M, Karczmar G, Yang C, et al. Semiquantitative analysis of dynamic contrast enhanced MRI in cancer patients: Variability and changes in tumor tissue over time. J Magn Reson Imaging 2004: 20: 122–128.

15. Rehman S, Jayson GC. Molecular imaging of antiangiogenic agents. Oncologist 2005: 10: 92–103.

16. Brekke C, Lundervold A, Enger PO, et al. NG2 expression regulates vascular morphology and function in human brain tumours. Neuroimage 2006: 29: 965–976.

17. Tofts PS. Modeling tracer kinetics in dynamic Gd-DTPA MR imaging. J Magn Reson Imaging 1997: 7: 91–101.

18. Menger MD, Jaeger S, Walter P, Feifel G, Hammersen F, Messmer K. Angiogenesis and hemodynamics of microvasculature of transplanted islets of Langerhans. Diabetes 1989: 38(Suppl. 1): 199–201.

19. Sandberg JO, Margulis B, Jansson L, Karlsten R, Korsgren O. Transplantation of fetal porcine pancreas to diabetic or normoglycemic nude mice. Evidence of a rapid engraftment process demonstrated by blood flow and heat shock protein 70 measurements. Transplantation 1995: 59: 1665–1669.

20. Morini S, Brown ML, Cicalese L, et al. Revascularization and remodelling of pancreatic islets grafted under the kidney capsule. J Anat 2007: 210: 565–577.

21. Mattsson G, Carlsson PO, Olausson K, Jansson L. Histological markers for endothelial cells in endogenous and transplanted rodent pancreatic islets. Pancreatology 2002: 2: 155–162.

22. McDonald DM, Choyke PL. Imaging of angiogenesis: From microscope to clinic. Nat Med 2003: 9: 713–725.

CHAPTER THREE

MONITORING NEOVASCULARIZATION OF INTRAPORTAL ISLET GRAFTS BY DYNAMIC CONTRAST ENHANCED MAGNETIC RESONANCE IMAGING

Nathaniel K. Chan, [1] Andre Obenaus,[2] Annie Tan, [1] Naoaki Sakata, [1,3] John Mace, [1] Ricardo Peverini, [1] Richard Chinnock, [1] Lawrence C. Sowers [1] and Eba Hathout [1,*]

[1]Islet Transplant Laboratory; Department of Pediatrics; and [2]Department of Radiation Medicine; Loma Linda University School of Medicine; Loma Linda, CA USA; [3]Division of Hepato-Biliary Pancreatic Surgery; Department of Surgery; Tohoku University Graduate School of Medicine; Sendai, Japan

Key words: islet transplantation, imaging, angiogenesis, islet blood flow, islet graft

Abbreviations: vWF, von Willebrand Factor; POD, post-operative day; DCE MRI, dynamic contrast-enhanced magnetic resonance imaging; AUC, area under the curve

*Correspondence to: Eba Hathout; Email: ehathout@llu.edu

Islets. 2009 Nov;1(3):249-255.

Abstract

Fifteen thousand youths are diagnosed yearly with type 1 diabetes mellitus. Pancreatic islet transplantation has been shown clinically to provide short-term (~1 year) insulin independence. However, challenges associated with early vascularization of transplanted islet grafts and long-term islet survival remain. We utilized dynamic contrast enhanced magnetic resonance imaging (DCE MRI) to monitor neovascularization of islets transplanted into the right lobe of the liver in a syngeneic mouse model. The left lobe received no islets and served as a control. DCE data were analyzed for temporal dynamics of contrast (gadolinium) extravasation and the results were fit to a Tofts two-compartment exchange model. We observed maximal right lobe enhancement at seven days post-transplantation. Histological examination up to 28 days was used to confirm imaging results. DCE-derived enhancement strongly correlated with immunohistochemical measures of neovascularization. To our knowledge these results are the first to demonstrate, using a FDA approved contrast agent, that DCE MRI can effectively and non-invasively monitor the progression of angiogenesis in intraportal islet grafts.

Introduction

Type 1 diabetes mellitus is a costly and growing medical problem, particularly within the pediatric population where an estimated 15,000 youths are diagnosed with type 1 diabetes annually.[1] The current standard of care involves insulin administered by injection or pump, but exogenous insulin treatment cannot perfectly control blood glucose levels despite advances in continuous glucose monitoring. Cumulative lifetime exposure to hyperglycemic episodes can lead to complications such as retinopathy, nephropathy, cardiovascular disease and peripheral neuropathy.[2,3] Islet cell transplantation has recently emerged as a promising therapeutic approach for providing long-term (>1 yr) insulin independence with the advent of the Edmonton Protocol.[4] More recently, an international trial showed that insulin independence could be achieved in more than 50% of transplanted patients, and that 80% of these patients were insulin-independent after one year.[5]

Despite these promising results, insulin independence is usually not sustainable, with 85–90% of patients requiring insulin injections by 5 years.[6] The failure of long-term insulin independence can be attributed to islet loss due to: (1) the immediate low rate of engraftment,[7,8] (2) progressive immune rejection,[9,10] (3) islet toxicity due to continued immunosuppressive drugs,[11-13] (4) low rate of engraftment due to extreme changes in the local tissue environment caused by the transplantation,[14] and (5) increased hypoxia from initial lack of islet vascularity.[15,16] In a healthy pancreas, islets account for 1–2% of pancreatic mass but receive 5–10% of blood flow.[17] After transplantation into the liver, islets are prone to hypoxia[18] with an estimated 50–70% of islets being lost in the immediate post-transplantation period that can then lead to functional impairment of the

remaining islets.[19-21] A tool to monitor the revascularization process is critical to advancing islet transplantation.

While standard MRI approaches can be used to detect the presence and size of islet grafts, visualization of islet graft revascularization remains unexplored. New imaging modalities, such as dynamic contrast-enhanced (DCE) MRI, are optimized to examine physiological parameters such as blood flow and capillary permeability and could be utilized to determine new vessel formation in transplanted islets. DCE MRI was first developed to characterize tumor vascularization[22,23] using rapid and repeated collection of images before, during, and after contrast administration, such as with gadolinium.[24,25] The temporal dynamics of contrast arrival within the vasculature and consequent leakage into the extra-vascular space have been modeled (two compartments) by Tofts et al.[26] The physiological parameters extracted using this model can be used to observe neovascularization at the transplant site.

Previously, we described a timeline for neovascularization after subcapsular kidney islet transplantation and demonstrated the feasibility of using DCE MRI to detect and quantify changes in vascularization over 28 days.[27,28] We have extended DCE MRI to monitor vascularization of intraportal islet transplants over 28 days post transplantation. Neovascularization was confirmed by immunohistochemical evaluation of transplanted islets and host liver tissue.

Results

DCE MRI and Vascularization of Intraportal Islet Grafts

MRI was used to monitor the progression of new vessel formation in the right liver lobe at post-operative day (POD) 3, 7, 14 and 28. High resolution T1-weighted imaging assisted in localization of the right (transplanted) and left (control) liver lobes (Fig. 3.1A), and was followed by placement of a single DCE slice at the same level. Rapidly acquired DCE images immediately before and after a single bolus injection of gadolinium (~0.04 cc) showed fast enhancement and slower wash out. Another high resolution T1 scan post-contrast indicated that equilibrium in enhancement was reached within 40 minutes after injection. The time course of right lobe enhancement in this subject at POD 14 showed that 4.3 minutes after contrast injection, a peak value of 2.2 was reached (Fig. 3.1B). The average time to peak contrast enhancement within the right liver varied significantly only between POD 3 and POD 14 ($p < 0.05$).

The average time to peak was 2.1 ± 0.2 mins at POD 3, 3.5 ± 0.2 mins at POD 7, 3.8 ± 0.6 mins at POD 14, and 2.8 ± 0.5 mins at POD 28 (Fig. 3.2). However, the magnitude and duration of the enhancement was dependent on the POD time point. Area under the curve (AUC) analysis showed marked increases at POD 7 and POD 28 (Fig. 3.2B) that trended towards significance ($p < 0.09$). The enhancement in the control lobes was not significantly different between POD periods, validating the use of the left liver lobe as a control. Similarly, no increased enhancement of muscle tissue was observed, validating consistent contrast injection dose and rate (data not shown). Comparing the maximum relative tissue concentration change between the right and left livers lobes

revealed a 30% increase at POD 7, followed by a small change of 8% at POD 14, and a resurgent increase to 26% at POD 28 (Fig. 3.2C).

New Vessel Formation Using vWF Immunostaining

Immunostaining for insulin verified the presence of insulin- containing islets at all time points (Fig. 3.3A–D). von Willebrand Factor (vWF) staining for new vessels (Fig. 3.3E–H) showed scant staining at POD 3 (Fig. 3.3E) with a larger increase in small new vessels in close proximity to islets at POD 7 (Fig. 3.3F). At POD 14, vessel numbers were decreased (Fig. 3.3G). However, by POD 28, the number of vWF positive vessels again increased (Fig. 3.3H). High magnification reveals typical peri-islet microvessel morphology at all time points (Fig. 3.3I–L).

Quantification of Islet Microvasculature

Quantification of vWF stained peri-islet microvessels showed the extent and time course of islet angiogenesis (Fig. 3.4). An average of 1.6 new vessels per islet was found at POD 3, 3.0 at POD 7, 2.3 at POD14 and 3.2 at POD 28. The number of microvessels at POD 7 and POD 28 were significantly increased compared to POD 3 by more than 80% ($p < 0.05$). There was no significant increase in new vessels at POD 14 as compared to POD 3.

Correlation of DCE MRI with Histological Vessel Quantification

The correlation between microvessel number and DCE MRI AUC was plotted and a linear least squares regression revealed a strong correlation ($r2 = 0.863$, $p < 0.001$). The positive slope of the regression line indicates that increases in contrast enhancement

are highly and significantly correlated with increases in new peri-islet microvessels (Fig. 3.5).

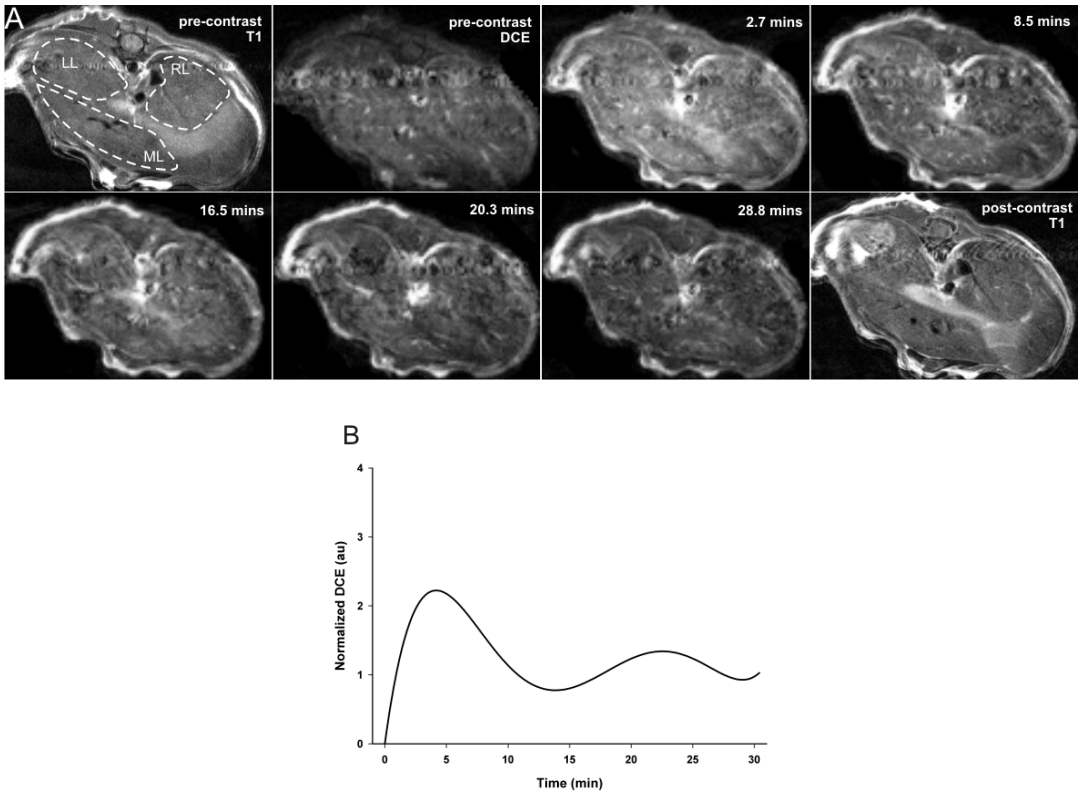

Figure 3.1. MRI visualization of murine liver lobes. (A) Representative T1-weighted transverse images at POD 14 of the multiple liver lobes before and after contrast administration. The right lobe (RL) received 800 islet equivalents (IEQ). The medial lobe (ML) and left lobe (LL) received no islets and were used as internal controls. Enhancement of various tissues including the right liver lobe occurs rapidly within the first five minutes, and slowly washes out. Forty minutes post-contrast, high resolution T1 shows equilibrated enhancement. (B) Average intensity of all pixels within the RL region of interest (ROI) over the duration of the DCE scan. The enhancement of the RL shows that the peak value of 2.2 occurs 4.3 minutes after contrast delivery.

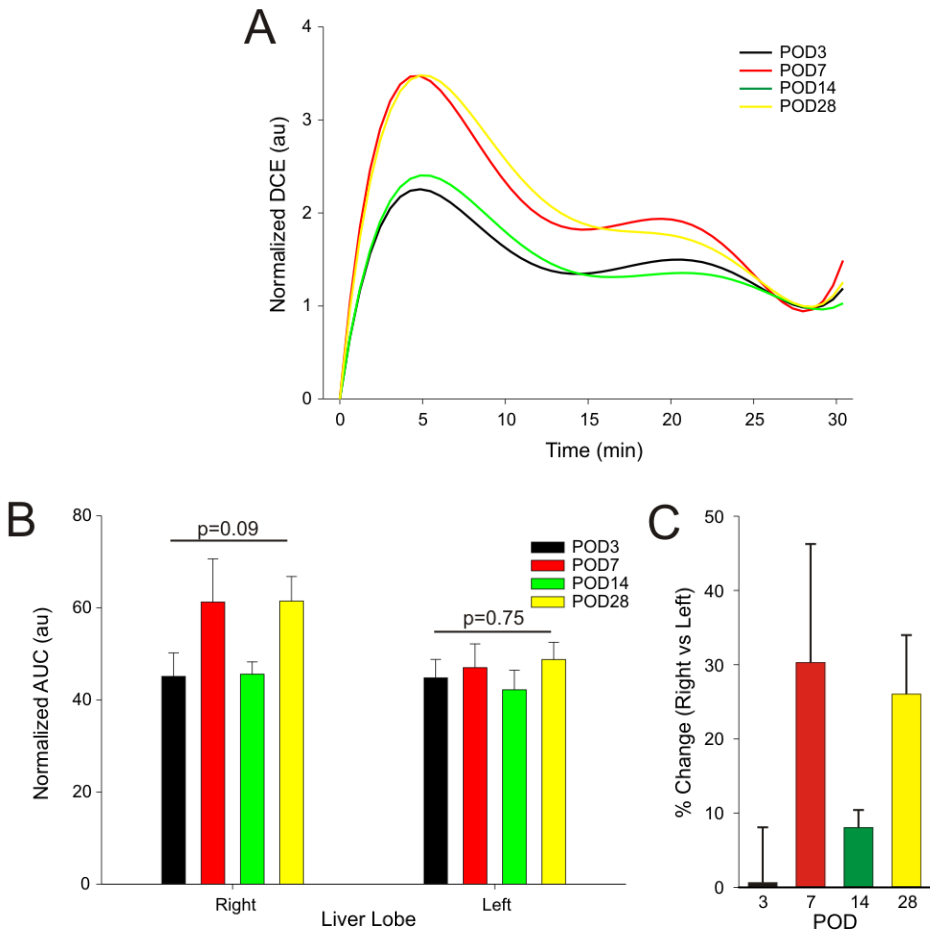

Figure 3.2. Temporal evolution of DCE MRI and neovascularization. (A) Averaged DCE curves of right liver lobes bearing islet grafts show an increase in enhancement at POD 7 and 28. (B) Area under the curve (AUC) analysis reflects the same general pattern of increased enhancement at POD 7 and 28, that was not observed in the untranplanted left liver lobes. There was a trend to significance (ANOVA, p = 0.09) for DCE increases in the right lobe but no significant temporal changes were found in the left liver. (C) The relative change in enhancement of right versus left lobes shows maximum enhancements at POD 7 and 28. (p = 0.09).

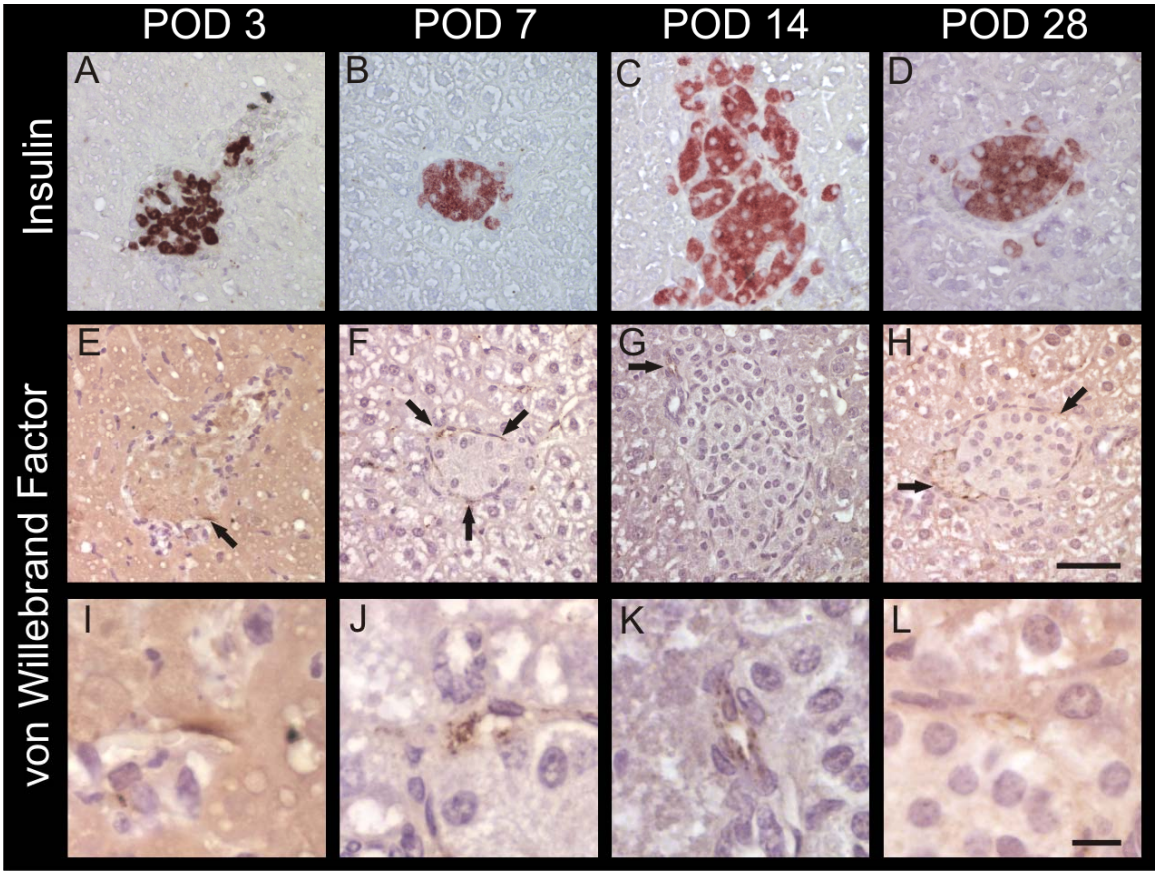

Figure 3.3. Histological assessment of islets and new vessel formation. (A–D) Islets were identified by insulin immunostaining. (E–H) Adjacent sections were immunostained for von Willebrand Factor (vWF) to identify newly formed blood vessels. Few peri-islet vessels stained positive for vWF at POD 3 but there were increased vessel numbers at POD 7 and 28. (Scale bar = 50 μm) (I–L) High magnification reveals typical microvessel morphology adjacent to the transplanted islets. (Scale bar = 10 μm).

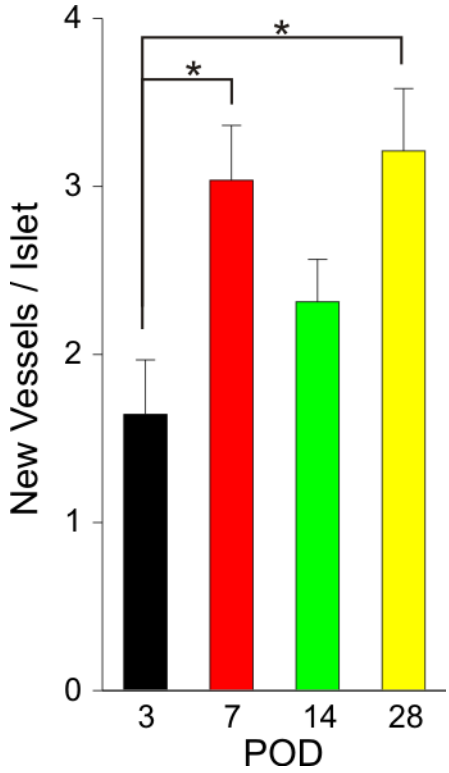

Figure 3.4. Time course of microvessel number. Quantification of peri-islet microvessels at each time point reveals significantly increased microvessel number at POD 7 and 28 compared to POD 3 (*$p < 0.05$).

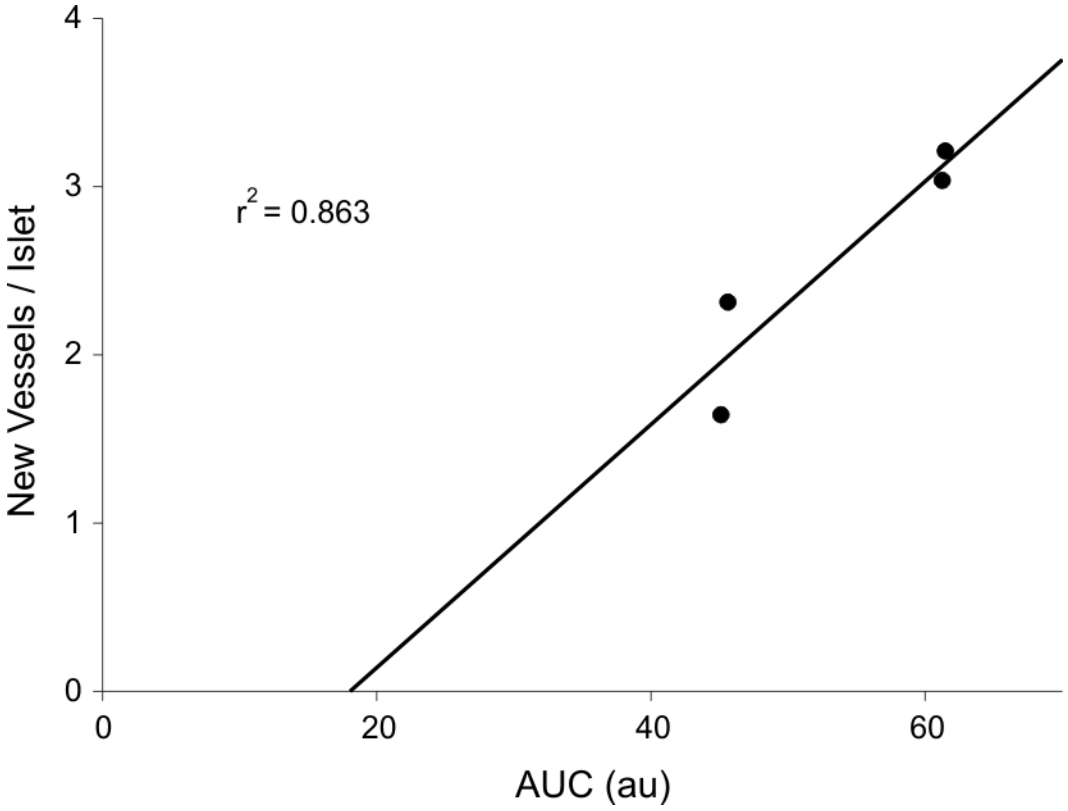

Figure 3.5. Correlation of DCE MRI and neovascular density. The number of new peri-islet microvessels plotted against AUC values derived from DCE MRI enhancement curves demonstrates a significant correlation coefficient of r2 = 0.863 ($p < 0.001$).

Discussion

To our knowledge, this is the first demonstration of DCE MRI using the FDA approved contrast agent Gd-DTPA to establish a timeline of vascularization in intraportal islet transplants. Based on this study, the authors claim the following novel findings: (1) non-invasive DCE MRI suggests a peak of new vessel formation in intraportal islet grafts at post-operative day (POD) 7, (2) immunohistochemical analysis shows a significantly increased number of new peri-islet vessels at POD 7 and POD 28 versus POD 3, and (3) DCE MRI findings strongly correlate with histology/immunohistochemistry results.

Peak enhancement at POD 7 is consistent with the increased rate of new vessel formation seen histologically by us as well as others.[29] Of note, the lack of von Willebrand staining within the islets is presumably due to an already mature though disrupted intra-islet donor-derived vasculature.[17] By POD 14, DCE-derived enhancement and new vessel numbers decreased, suggestive of a mature islet vasculature. This finding in our non-diabetic model is consistent with the timeline of revascularization described in a diabetic model.[30] There was a secondary elevated enhancement in the right liver again at POD 28. Though it was not statistically significant, the increased enhancement appears to be related to the process of angiogenesis as histological assessment revealed a concordant increase in new vessel numbers. Previous subcapsular studies[27,28] found that similar numbers of animals resulted in significant DCE changes reflective of angiogenesis while in the current study there was a clear trend towards increased DCE that did not reach significance. A potential explanation could be that the subcapsular transplants were confined to focal regions in contrast to the intraportal transplants that

where spread out throughout the entire liver, thus making the angiogenic process more diffuse.

We considered whether islet death as opposed to angiogenesis was the cause of increased enhancement as islet number slowly wanes with time.[10,31] A decreased islet mass due to necrosis and/or apoptosis at POD 28 might have caused an inflammatory response and resulted in increased vessel permeability, leading to the increased enhancement seen in the right lobe. However, in another study, histological staining of islet grafts for apoptosis (TUNEL), necrosis (H&E), and HIF-1α revealed essentially no positive stain at this late POD 28 time point [32]. Whether the islet neovascularization process is different in non-diabetic mice, whether there is a paring back of islet vasculature in between the two phases of angiogenesis, or whether this reduction may be responsible for the late second phase are all yet to be determined.

It is currently unclear as to the basis for the bi-phasic response (DCE and vessel number) after intraportal transplantation. Several potential reasons include: (1) use of a non-diabetic model, where hyperglycemia-associated stimuli may be missing, (2) secondary signaling from pro-angiogenic factors might be transiently blunted by hypoxia-inducible factors at POD 14, and (3) accelerated but unsustained angiogenesis in intraportal transplantation (7 days earlier than subcapsular)[27,28] may potentially lead to a secondary local hypoxic event that further stimulates angiogenesis. However, only future work evaluating the molecular angiogenic profiles at these time points will be able to definitively resolve this interesting finding.

The use of untransplanted liver lobes as controls helped to avoid intersubject variability and was justified as the dynamics of enhancement did not vary significantly

over time. Any effects that may have been caused by the transient (~1 min) ischemia from clamping of the left portal vein branches during islet transplantation were not evident on DCE MRI at POD 3 and beyond. One potential limitation of infusing islets into only the right liver lobe was the possibility that initial portal thrombosis from islet clusters and/or macrophages would lower the blood flow through the right lobe and concomitantly increase flow to the other lobes.[33] Such a differential in flow could have been manifest as decreased delivery of contrast agent to and decreased enhancement of the right lobe. Activation of the extrinsic coagulation pathways may have also been another source of right lobe specific thrombosis.[34] However, by the earliest imaging time point at POD 3, no right lobe thromboses were evident as right lobe enhancement was statistically no different than the control lobe, thus validating the lobe-specific transplant model.

Another advantage of this approach is its independence from islet labeling. The clinical utility of MRI in islet transplantation has recently been demonstrated,[35] but visualization of islets required labeling with superparamagnetic iron oxide (SPIO). Micro-positron emission tomography (PET) is another imaging modality that has been used to track islet survival.[36-38] However, neither PET nor MRI without contrast is able to resolve the details of vascular structures. MRI with an experimental long circulating contrast agent (PGC-GdDTPA-F) has been used to monitor the vascular changes around native pancreatic islets.[39] In earlier studies we have established a timeline for islet revascularization in subcapsular kidney grafts.[27,28] In an attempt to visualize intraportal islets *in vivo*, islets in this study were co-cultured with Feridex overnight before transplantation. However, labeling efficiency without membrane permeabilization (eg

electroporation, polylysine) was seen to be poor and individual transplanted islets were difficult to detect with T2-weighted scans (data not shown). Thus only the T1-weighted scans have been reported here. The possible confounding effect of negative contrast labeled islets on positive intravascular contrast detection did not appear to be an issue due in part to the low labeling efficiency and the fact that the negative contrast effect of Feridex is strongest with T2-weighted scans. The T1 effect of Feridex did not seem to be significant in this study because the enhancement of transplanted and untransplated lobes was equal at an early time point (POD3) (Fig. 3.2) before revascularization. The concentration of Feridex in islets was very low relative to the gadolinium concentration in the whole liver lobe.

In this study we have shown that MRI with a clinical positive contrast agent can be used to follow the vascularization of syngeneic murine islets transplanted into the liver. Whole lobe analysis allows this technique to be independent of the ability to visualize individual islets *in vivo*. These studies suggest that DCE MRI might eventually be applicable in humans and useful in evaluating therapeutic strategies for increasing the efficiency of engraftment in clinical islet transplantation.

Material and Methods

Animals

Adult female Balb/c mice weighing 25–30 g were purchased (Charles River, Wilmington, MA) and housed under specific pathogen-free conditions with a 12-hr light/dark cycle and had free access to food and water. All care and handling of animals

was in accordance with Loma Linda University Institutional Animal Care Use Committee which approved all experimental protocols.

Islet Transplantation

Islets were isolated by collagenase digestion of the pancreas and separated from exocrine tissue by discontinuous Ficoll density gradient centrifugation and then hand-picked as previously described.27 Iron labeling of islets was performed by overnight co-culture of freshly isolated islets in Feridex (Advanced Magnetics Inc., Cambridge MA)-supplemented medium at 200 μg iron/ml. Under general inhalation anesthesia (2% isoflurane), a midline incision was made in recipient mice, the bowel was moved out of the abdominal cavity to expose the portal vein at the level of hepatic hilar to ileocecal veins. The left portal vein was temporarily clamped, the ileocecal vein was punctured with a 25-gauge needle (Becton Dickinson, NJ, USA) and 800 syngeneic islet equivalents (IEQ = islets with a diameter of 150 μm) were slowly injected into the right liver lobe. The needle was pulled out with pressure from a cotton swab to stop bleeding. Animals were allowed to recover for 72 hours prior to the first imaging time point.

Magnetic Resonance Imaging (MRI)

MRI was performed at 3 (n = 6), 7 (n = 4), 14 (n = 5) and 28 (n = 4) days post transplantation (POD). Each mouse was imaged prior to and after-contrast injection using a T1-weighted sequence of the entire liver. DCE MRI was performed on a slice through which both right and left liver lobes were visible. All MRI data were collected on a Bruker Advance 11.7 T MRI (8.9 cm bore) with a 3.0 cm (ID) volume radiofrequency

coil (Bruker Biospin, Billerica MA). Mice were lightly anesthetized using isoflurane (3% induction, 1% maintenance). A tail vein catheter was inserted and fastened to the tail for infusion of gadolinium DTPA contrast (Gd-DTPA, -BMA, Gadodiamide, 0.8 mmol/kg, Omniscan, Amersham Health, Princeton NJ). Body temperature was maintained at 35–37 ± 1°C using a thermostat-controlled heated water cushion placed under the mouse while respiration was monitored with a MR-compatible pressure transducer on a Biopac MP150 (Goleta CA).

A high resolution pre/post-contrast T1 composed of a TR/ TE of 837/10 ms, a 256^2 matrix, 3 cm field of view (FOV), and 4 averages for a total acquisition time of 14 minutes. Twenty coronal slices were collected with a 0.8 mm thickness and interleaved by 0.8 mm. These T1 images were visually evaluated to identify the liver lobes. A single DCE acquisition slice was then placed through a section of liver that included the transplanted right lobe. The DCE sequence acquired one image slice through the liver using a TR/TE = 250/6.4 ms, 128^2 matrix, 3 cm FOV, one average for an acquisition time of 32 sec/image and a total acquisition time of 32 minutes with 60 images collected.

MRI Analysis

DCE analysis utilized the temporal dynamics of contrast enhancement that were quantified using JIM software (Thorpe Waterville, UK). Briefly, regions of interest (ROIs) (right liver, left liver and muscle) were identified on the DCE images based on T1 images (Fig. 1). Kinetic analysis used a bidirectional two-compartment model based on the equations of Tofts et al.[26] Briefly, contrast agent that is injected into the blood pool extravasates into different tissues with various permeabilities. This process can be

described by equations that model the dynamics of contrast agent exchange back and forth between the blood and tissue compartments. DCE MRI tissue gadolinium concentration curves extracted from JIM software were normalized for inter- and intra-animal comparisons and then averaged and curve fit. Area under the curve (AUC) values were calculated by integrating the area using the trapezoidal method.

Histology and Immunohistochemistry

After imaging, the liver was recovered and placed in 10% formalin for 24 hrs and then the right lobe(s) was embedded in paraffin. The orientation of liver tissue blocks was kept consistent and five μm serial sections were taken at four different levels through the lobes at 400 μm intervals. Sections were deparaffininized in xylene and hydrated. Sections were stained with Hematoxylin and Eosin (H&E) and immunohistochemistry for insulin and von Willebrand Factor (anti-vWF) was performed to identify the presence of insulin in the islets and peri-islet neovasculature.40,41 To restore antigen immunoreactivity for anti-vWF, tissue was treated with Proteinase K (Dako, Carpinteria, CA) for 2 minutes followed by blockade of endogenous peroxidase activitiy by treatment of 0.1% hydrogen peroxide for 30 minutes. Nonspecific binding was blocked with 10% goat serum for 30 minutes. Specimens were incubated with either the guinea pig anti-insulin antibody (1:100; Dako) or rabbit anti-vWF (1:500; Abcam, Cambridge, MA) for 90 minutes at room temperature. Biotinylated anti-rabbit IgG antibody treatment for 30 minutes was followed by streptavidin-conjugated horseradish peroxidase treatment for an additional 30 minutes (Vectastain Elite ABC kit; Vector Laboratories, Burlingame, CA). Bound peroxidase was developed with 3-3'-diaminobenzidine (DAB: brown; Dako) for

vWF or aminoethylcarbozole chromogen (AEC+:red; Dako) for insulin and counterstained with hematoxylin.

Immunohistochemical Analysis

Insulin-postive islets were identified in liver sections by brightfield microscopy, images were captured (Zeiss Axio Imager A1) and islet area was manually outlined (ImageJ, NIH). Islets larger than 1,800 μm2 underwent microvessel quantification on subsequent vWF stained sections (n = 14 at POD3, n = 28 at POD 7, n = 64 at POD14, n = 19 at POD28). New microvessels that stained positive for vWF were counted by a blinded observer at higher magnification (200– 400x). Inclusion criteria for islet-specific microvessels were: (1) localization, vessels were in contact with or within the islet and (2) morphology, vessels must be less than 40 μm along the longest axis.

Statistical Analysis

Statistical evaluation including repeated measures ANOVA (RM ANOVA) was performed using Sigmastat software (SPPS, Chicago IL) and differences among experimental groups were considered significant for $p < 0.05$. Pairwise comparisons were made using the Holm-Sidak method and post-hoc t-tests. Data were expressed as the mean ± standard error of the mean (SEM).

Acknowledgements

We are grateful for the technical assistance provided by John Chrisler, Pete Hayes and Tom Lechuga. Special thanks also to Dr. William Pearce. This work was supported by NIH/NIDDK grant number 1-R01-DK077541-03 (E.H.).

References

1. Centers for Disease Control and Prevention. National diabetes fact sheet: general information and national estimates on diabetes in the United States, 2007 Atlanta, GA: U.S. Department of Health and Human Services, Centers for Disease Control and Prevention, 2008.

2. Bailes BK. Diabetes mellitus and its chronic complications. AORN J 2002; 76:266-76.

3. Bloomgarden ZT. Diabetes complications. Diabetes Care 2004; 27:1506-14.

4. Shapiro AM, Lakey JR, Ryan EA, Korbutt GS, Toth E, Warnock GL, et al. Islet transplantation in seven patients with type 1 diabetes mellitus using a glucocorticoid-free immunosuppressive regimen. N Engl J Med 2000; 343:230-8.

5. Shapiro AM, Ricordi C, Hering BJ, Auchincloss H, Lindblad R, Robertson RP, et al. International trial of the Edmonton protocol for islet transplantation. N Engl J Med 2006; 355:1318-30.

6. Ryan EA, Paty BW, Senior PA, Bigam D, Alfadhli E, Kneteman NM, et al. Five-year follow-up after clinical islet transplantation. Diabetes 2005; 54:2060-9.

7. Bennet W, Groth CG, Larsson R, Nilsson B, Korsgren O. Isolated human islets trigger an instant blood mediated inflammatory reaction: implications for intraportal islet transplantation as a treatment for patients with type 1 diabetes. Ups J Med Sci 2000; 105:125-33.

8. van der Windt DJ, Bottino R, Casu A, Campanile N, Cooper DK. Rapid loss of intraportally transplanted islets: an overview of pathophysiology and preventive strategies. Xenotransplantation 2007; 14:288-97.

9. Chen X, Zhang X, Larson CS, Baker MS, Kaufman DB. In vivo bioluminescence imaging of transplanted islets and early detection of graft rejection. Transplantation 2006; 81:1421-7.

10. Evgenov NV, Medarova Z, Pratt J, Pantazopoulos P, Leyting S, Bonner-Weir S, Moore A. In vivo imaging of immune rejection in transplanted pancreatic islets. Diabetes 2006; 55:2419-28.

11. Desai NM, Goss JA, Deng S, Wolf BA, Markmann E, Palanjian M, et al. Elevated portal vein drug levels of sirolimus and tacrolimus in islet transplant recipients: local immunosuppression or islet toxicity? Transplantation 2003; 76:1623-5.

12. Fiorina P, Secchi A. Pancreatic islet cell transplant for treatment of diabetes. Endocrinol Metab Clin North Am 2007; 36:999-1013.

13. Korsgren O, Lundgren T, Felldin M, Foss A, Isaksson B, Permert J, et al. Optimising islet engraftment is critical for successful clinical islet transplantation. Diabetologia 2008; 51:227-32.

14. Barshes NR, Wyllie S, Goss JA. Inflammation-mediated dysfunction and apoptosis in pancreatic islet transplantation: implications for intrahepatic grafts. J Leukoc Biol 2005; 77:587-97.

15. Mattsson G, Jansson L, Carlsson PO. Decreased vascular density in mouse pancreatic islets after transplantation. Diabetes 2002; 51:1362-6.

16. Carlsson PO, Palm F, Mattsson G. Low revascularization of experimentally transplanted human pancreatic islets. J Clin Endocrinol Metab 2002; 87:5418-23.

17. Brissova M, Powers AC. Revascularization of transplanted islets: can it be improved? Diabetes 2008; 57:2269-71.

18. Sakata N, Hayes P, Tan A, Chan N, Mace J, Peverini R, et al. MRI Assessment of Ischemic Liver Following Intraportal Islet Transplantation. Transplantation 2009; 87.

19. Davalli AM, Ogawa Y, Ricordi C, Scharp DW, Bonner- Weir S, Weir GC. A selective decrease in the beta cell mass of human islets transplanted into diabetic nude mice. Transplantation 1995; 59:817-20.

20. Davalli AM, Scaglia L, Zangen DH, Hollister J, Bonner-Weir S, Weir GC. Vulnerability of islets in the immediate posttransplantation period. Dynamic changes in structure and function. Diabetes 1996; 45:1161-7.

21. Mattsson G, Jansson L, Nordin A, Andersson A, Carlsson PO. Evidence of functional impairment of syngeneically transplanted mouse pancreatic islets retrieved from the liver. Diabetes 2004; 53:948-54.

22. Cuenod CA, Fournier L, Balvay D, Guinebretiere JM. Tumor angiogenesis: pathophysiology and implications for contrast-enhanced MRI and CT assessment. Abdom Imaging 2006; 31:188-93.

23. Medved M, Karczmar G, Yang C, Dignam J, Gajewski TF, Kindler H, et al. Semiquantitative analysis of dynamic contrast enhanced MRI in cancer patients: Variability and changes in tumor tissue over time. J Magn Reson Imaging 2004; 20:122-8.

24. Choyke PL, Dwyer AJ, Knopp MV. Functional tumor imaging with dynamic contrast-enhanced magnetic resonance imaging. J Magn Reson Imaging 2003; 17:509-20.

25. Cheng HL, Chen J, Babyn PS, Farhat WA. Dynamic Gd-DTPA enhanced MRI as a surrogate marker of angiogenesis in tissue-engineered bladder constructs: a feasibility study in rabbits. J Magn Reson Imaging 2005; 21:415-23.

26. Tofts PS. Modeling tracer kinetics in dynamic Gd-DTPA MR imaging. J Magn Reson Imaging 1997; 7:91-101.

27. Hathout E, Sowers L, Wang R, Tan A, Mace J, Peverini R, et al. In vivo magnetic resonance imaging of vascularization in islet transplantation. Transpl Int 2007; 20:1059-65.

28. Hathout E, Chan NK, Tan A, Sakata N, Mace J, Pearce W, et al. In vivo imaging demonstrates a time-line for new vessel formation in islet transplantation. Pediatr Transplant 2008; 13:892-7

29. Jones GL, Juszczak MT, Hughes SJ, Kooner P, Powis SH, Press M. Time course and quantification of pancreatic islet revascularization following intraportal transplantation. Cell Transplant 2007; 16:505-16.

30. Griffith RC, Scharp DW, Hartman BK, Ballinger WF, Lacy PE. A morphologic study of intrahepatic portalvein islet isografts. Diabetes 1977; 26:201-14.

31. Kriz J, Jirak D, Girman P, Berkova Z, Zacharovova K, Honsova E, et al. Magnetic resonance imaging of pancreatic islets in tolerance and rejection. Transplantation 2005; 80:1596-603.

32. Sakata N, Hayes P, Tan A, Chan NK, Mace J, Peverini R, et al. MRI assessment of ischemic liver after intraportal islet transplantation. Transplantation 2009; 87:825-30.

33. Montolio M, Tellez N, Soler J, Montanya E. Role of blood glucose in cytokine gene expression in early syngeneic islet transplantation. Cell Transplant 2007; 16:517-25.

34. Contreras JL, Eckstein C, Smyth CA, Bilbao G, Vilatoba M, Ringland SE, et al. Activated protein C preserves functional islet mass after intraportal transplantation: a novel link between endothelial cell activation, thrombosis, inflammation and islet cell death. Diabetes 2004; 53:2804-14.

35. Toso C, Vallee JP, Morel P, Ris F, Demuylder-Mischler S, Lepetit-Coiffe M, et al. Clinical magnetic resonance imaging of pancreatic islet grafts after iron nanoparticle labeling. Am J Transplant 2008; 8:701-6.

36. Kim SJ, Doudet DJ, Studenov AR, Nian C, Ruth TJ, Gambhir SS, McIntosh CH. Quantitative micro positron emission tomography (PET) imaging for the in vivo determination of pancreatic islet graft survival. Nat Med 2006; 12:1423-8.

37. Eich T, Eriksson O, Sundin A, Estrada S, Brandhorst D, Brandhorst H, et al. Positron emission tomography: a real-time tool to quantify early islet engraftment in a preclinical large animal model. Transplantation 2007; 84:893-8.

38. Toso C, Zaidi H, Morel P, Armanet M, Andres A, Pernin N, et al. Positron-emission tomography imaging of early events after transplantation of islets of Langerhans. Transplantation 2005; 79:353-5.

39. Medarova Z, Castillo G, Dai G, Bolotin E, Bogdanov A, Moore A. Noninvasive magnetic resonance imaging of microvascular changes in type 1 diabetes. Diabetes 2007; 56:2677-82.

40. McDonald DM, Choyke PL. Imaging of angiogenesis: from microscope to clinic. Nat Med 2003; 9:713-25.

41. Miao G, Mace J, Kirby M, Hopper A, Peverini R, Chinnock R, et al. In vitro and in vivo improvement of islet survival following treatment with nerve growth factor. Transplantation 2006; 81:519-24.

CHAPTER FOUR

HYPERBARIC OXYGEN THERAPY IMPROVES EARLY POSTTRANSPLANT ISLET FUNCTION

Naoaki Sakata[a,b], Nathaniel K. Chan[a], Robert P. Ostrowski[c], John Chrisler[a], Pete Hayes[d], Sonny Kim[d], Andre Obenaus[d,e], John H. Zhang[c] and Eba Hathout[a]

[a]Department of Pediatrics, Islet Transplant Laboratory, Loma Linda University School of Medicine, Loma Linda, CA 92354, USA; [b]Division of Hepato-Biliary Pancreatic Surgery, Department of Surgery, Tohoku University Graduate School of Medicine, Sendai, Miyagi 980-8574, Japan; [c]Department of Physiology and Pharmacology, Loma Linda University School of Medicine, Loma Linda, CA 92354, USA; [d]Department of Radiation Medicine, Loma Linda University School of Medicine, Loma Linda, CA 92354, USA; and [e]Department of Radiology, Loma Linda University School of Medicine, Loma Linda, CA 92354, USA

Running Title: HBO affects transplanted islet function

Key words: Islet transplantation, HBO treatment, HIF-1α, MRI, VEGF

Corresponding author:
Eba Hathout, MD
Professor and Chief, Division of Pediatric Endocrinology, Director, Department of Pediatrics, Pediatric Diabetes Center and Islet Transplant Laboratory
Loma Linda University School of Medicine
11175 Campus Street, Coleman Pavilion A1120R
Loma Linda, CA 92354, USA.
Tel: +1 909 558 4773;
fax: +1 909 558 0408;
e-mail: ehathout@llu.edu

Pediatric Diabetes. 2010 Nov;11(7):471-8.

Abstract

Objective: This study investigates the therapeutic potential of hyperbaric oxygen therapy (HBO) in reducing hypoxia and improving engraftment of intraportal islet transplants by promoting angiogenesis.

Methods: Diabetic BALB/c mice were transplanted with 500 syngeneic islets intraportally and received six consecutive twice-daily HBO treatments (n = 9; 100% oxygen for 1 h at 2.5 atmospheres absolute) after transplantation. Dynamic contrast-enhanced magnetic resonance imaging (DCE MRI) was used to assess new vessel formation at postoperative days (POD) 3, 7, and 14. Liver tissue was recovered at the same time points for correlative histology, including: hematoxylin and eosin, hypoxia-inducible factor (HIF1α), Terminal deoxynucleotidyl transferase (TdT)-mediated dUTP-biotin nick end labeling (TUNEL), vascular endothelial growth factor (VEGF), and von Willebrand Factor immunohistochemistry.

Results: HBO therapy significantly reduced HIF-1α, TUNEL and VEGF expression in islets at POD 7. In the non-HBO transplants, liver enhancement on DCEMRI peaked at POD 7 consistent with less mature vasculature but this enhancement was suppressed at POD 7 in the HBO-treated group. The number of new peri-islet vessels at POD 7 was not significantly different between HBO and control groups.

Conclusion: These results are consistent with a hyperbaric oxygen-mediated decrease in hypoxia that appeared to enhance vessel maturation in the critical days following intraportal islet transplantation.

Introduction

Advances in islet transplantation depend upon prolongation of islet graft viability with a robust insulin response. Although intraportal islet transplantation has been the most successful route clinically (1–3), approximately 60% of islets are lost following intraportal infusion (4, 5). Therefore, non-invasive monitoring of transplanted islets is critical for understanding islet health and for deciding adjuvant therapeutic strategies.

Recently, non-invasive examination of transplanted islets has been performed by a variety of methods including magnetic resonance imaging (MRI) (6, 7). In addition to structural imaging, we have reported the effectiveness of dynamic contrast-enhanced MRI (DCE MRI) for assessment of angiogenesis after renal subcapsular transplantation of islets (8, 9). We have also demonstrated that DCE MRI can reflect islet neovascularization after intraportal islet transplantation (10).

A major reason contributing to early graft loss is islet hypoxia (11, 12). Transplanted islets are avascular at the time of transplantation and suffer from hypoxia until revascularization occurs at 1–2 wk after transplantation (8, 13). In a previous study, we found that hypoxia-inducible factor-1α (HIF- 1α) expression was increased in islets after renal subcapsular transplantation in association with β cell death and decreased insulin production (14), which was reversible when revascularization was established. Of note, these transient decrements in islet function could be mitigated by hyperbaric oxygen (HBO) treatment (14). HBO has been used therapeutically in various other clinical and experimental conditions, particularly those associated with increased hypoxia.

In the present study, we focus on intraportal islet transplantation and the effect of HBO treatment in reducing islet hypoxia and apoptosis, improving islet graft function

and its effectiveness to enhance graft neovascularization.

Materials and methods

Animals

BALB/c female mice (22–27 g, Charles River Laboratories. Inc., Boston, MA, USA) were used as both donors and recipients. The mice were housed under pathogen-free conditions with a 12-h light cycle and free access to food and water. All animal care and treatment procedures were approved by the Institutional Animal Care Use Committee.

Induction of Diabetes in Recipient Mice

Streptozotocin (STZ, 200 mg/kg/mouse, Sigma- Aldrich, St Lois, MO, USA) was injected intraperitoneally and blood glucose levels were measured by Accu-Chek Advantage glucose monitors (Roche, Indianapolis, IN, USA). Diabetes was diagnosed when the blood glucose level was greater than 13.8 mmol/L.

Islet Isolation

Murine islets were isolated by collagenase (collagenase V, Sigma-Aldrich) digestion, separation by Ficoll (Sigma-Aldrich) discontinuous gradients and purification as previously described (15).

Islet Function and Viability

Islets for *in vitro* assays (n = 10 islets) were incubated for 2 h in RPMI 1640 medium containing 3.3 mmol/L glucose (preincubation). Low glucose (3.3 mmol/L)

incubation for 30 min was then followed by high glucose (16.7 mmol/L) incubation for an additional 30 min. Supernatants were collected after each incubation and insulin content was extracted from the islets with acid ethanol. Insulin release and insulin content were measured using an insulin enzymelinked immunosorbent assay (ELISA) kit (Linco,MO, USA) and the stimulation index (SI) was calculated by dividing the insulin released in high glucose by insulin released in low glucose. The percentage of viable islets were examined by staining 50 islets with SYTO® green (Invitrogen, Carlsbad, CA, USA) and ethidium bromide (Sigma-Aldrich), calculating the viability ratio (viable islet cells/(viable islet cells + dead islet cells)× 100) of each islet using Image J (v1.37, National Institutes of Health, Bethesda, MD, USA) and calculating the average (16).

Islet Transplantation and Hyperbaric Oxygen (HBO) Treatment

Cultured syngeneic islets 500 islet equivalents, (IEQ = 150 μm) were transplanted via the portal vein into diabetic mice (17). IEQ's were calculated by microscopically measuring islet size where we collected 133–200 μm sized islets but rejected islets greater than 267 μm in size (18). We considered 500 IEQ a marginal islet mass for restoring normoglycemia based on our previous results that showed only 20% of mice achieving normoglycemia with 500 IEQ whereas 75% of the mice with 800 IEQ reached normoglycemia (19). Islet transplanted mice were divided into two groups: (i) no HBO treatment (controls: n = 10), and (ii) HBO treatment (n = 9). HBO treatment with 100% oxygen for 1 h at 2.5 atmospheres absolute (ATA) was initiated immediately posttransplantation and then twice daily for a total of six exposures (0, 12, 24, 36, 48, and 60 h). This HBO protocol was based on our previous study (14). Mice were placed in a

hyperbaric chamber (Model 1300B, Sechrist Industries In., Anaheim, CA, USA) with a compression rate of 5 psi/min (psi: pound-force per square inch, 1 ATA = 14.223 psi) and oxygen flow at a rate of 22 L/min. Accumulation of CO2 was prevented by calcium carbonate crystals. No complications because of HBO treatment were observed.

MRI Acquisition

MRI was conducted at postoperative days (POD) 3, 7, and 14 according to our previously published methods (8). Briefly, mice were lightly anesthetized using isoflurane and a tail vein catheter was inserted for infusion of gadolinium DTPA contrast [Gadodiamide hydrate (Gd-DTPA-BMA), 0.1 mmol/kg body weight, Omniscan, Amersham Health, Princeton, NJ, USA]. Body temperature was maintained at 36 ± 1◦C and respiration was monitored with an MR-compatible pressure transducer (Biopac MP150, Goleta, CA, USA). Imaging was performed on a Bruker Advance 11.7 T MRI (Bruker Biospin, Billerica, MA, USA) with a 3.0 cm internal diameter (ID) volume radiofrequency coil. The pre/postcontrast T1 was composed of a repetition time/echo time (TR/TE) of 832/10 ms, a 256^2 matrix, 3-cm field of view (FOV), and two averages for a total acquisition time of 14 min. The standard T1 sequences collected 20 coronal slices that were 0.75-mm thick and interleaved by 0.75 mm. The DCE sequence was a rapid image acquisition that acquired one image slice through the right and left liver lobes with the following parameters: TR/TE = 250/6.4 ms, 128^2 matrix, 3-cm FOV, one average for an acquisition time of 32 s/image and a total acquisition time of 32 min with 60 images collected. The contrast agent was injected 2 min after the start of the DCE MRI.

MRI Analysis

DCE analysis utilized the temporal dynamics of contrast enhancement that were quantified using jim software (Xinapse Systems, Thorpe Waterville, Northamptonshire, UK) as previously described (8). Briefly, regions of interest (20) (right liver, left liver, and muscle) were identified on the DCE images and kinetic analysis used a bi-directional two compartment model (time and area of enhancement) based on the equations of Tofts (21). DCE MRI tissue Gd concentration curves were extracted and normalized for inter- and intra-animal comparisons and then curve fit. Areas under the curve (AUC) values were calculated by integrating using the trapezoidal method using SigmaStat (Systat Software, Inc. Chicago, IL, USA). The AUC ratio at POD 7 and 14 vs. POD 3 [= (AUC at POD 7/AUC at POD 3) and (AUC at POD 14/AUC at POD 3)] were used to compare HBO and control groups.

Histological Assessment

Liver specimens were acquired from four, five, and six mice at POD 3, 7, and 14, respectively. The fixed livers were embedded in paraffin and cut in 5-μm thick sections. Specimens were stained for hematoxylin and eosin (H & E) for cellular changes, insulin immunohistochemistry to identify islets, HIF-1α to determine hypoxia, vascular endothelial growth factor (VEGF) and von Willebrand Factor (vWF) for newly formed blood vessels. For vWF staining, specimens were treated with Proteinase K (Dako, Carpiteria, CA, USA). Primary antibodies were guinea pig anti-insulin antibody (Dako) diluted with 1:100, goat anti-HIF-1α antibody (Santa Cruz Inc., Santa Cruz, CA, USA) diluted with 1:25, goat anti-VEGF antibody Santa Cruz Inc.) diluted with 1:50 and rabbit

anti-vWF (Abcam, Cambridge, MA, USA) diluted with 1:500. After incubating with biotinylated secondary Immunoglobulin G antibody (Vector Laboratories, Burlingame, CA, USA and Santa Cruz Inc.), a peroxidase substrate solution containing 3,3'-diaminobenzidine (DAB, brown for HIF-1α, Dako) or aminoethylcarbazol (AEC)+ (Red for insulin, Dako) was used for visualization and counterstained with hematoxylin (14). Apoptosis was detected by the Terminal deoxynucleotidyl transferase (TdT)-mediated dUTP-biotin nick end labeling (TUNEL) method using an in situ apoptosis detection kit (Promega, Madison, WI, USA). Sections were treated with proteinase K and incubated with TdT enzyme for 60 min at 37°C. After washing in PBS, the sections were further incubated with streptavidin horseradish peroxidase (HRP) solution and visualized with DAB (14).

Islet cells and surrounding liver tissue were assessed for necrosis (defined as destruction of cell structure with granulation, H & E), apoptosis (TUNEL), and hypoxia (HIF-1α). Expression of VEGF in islet cells was also examined. Islet cell apoptosis was expressed as the percentage of TUNEL positive islets relative to total islets. The proportion of hypoxic islet cells was expressed as percentage of HIF-1α positive cells in an islet. Expression of VEGF in islet cells was indicated as percentage of VEGF positive cells in an islet. Necrotic islet cells, hypoxia, apoptosis, and necrosis of the surrounding liver tissue were microscopically scored as zero (absent) or one (present). Newly formed vessels around islets were calculated by counting vWF-positive lumens (brown) adjacent to the islets. The number of islets at POD 3, 7, and 14 were 67 (from 2 mice), 51 (from 3 mice) and 33 (from 3 mice) in HBO group, respectively, and 50 (from 2 mice), 56 (from 2 mice), and 75 (from 3 mice) in the control group at POD 3, 7, and 14.

Blood Glucose, Percentage and Day of Normoglycemia, Serum Insulin Levels and Glucose Tolerance Test (GTT)

Blood glucose was measured at POD 0 (pretransplant) and POD1, 2, 3, 5, 7, 10, and 14. Serum insulin and glucose tolerance test (GTT) were measured at POD 7 and 14. Days to and percentage of normoglycemia were calculated using a blood glucose level of ≤8.3 mmol/L as normoglycemia. Intraperitoneal GTT were performed at POD 7 and 14 by overnight fasting for 10 h and then injecting mice with a 2.0 g/kg body weight of glucose solution followed by tail vein blood samples at 0, 15, 30, 60, 90, and 120 min after injection. Glucose level change was expressed as area under the curve (AUC: mmol/L X min). Serum insulin and C-peptide levels were not measured after glucose stimulation.

Blood glucose levels were measured by Accu-Chek Advantage glucose monitors and serum insulin was measured with a rat/mouse insulin ELISA kit.

Statistical analysis

All the data were expressed as mean ± standard error of the mean. Analysis of variance was performed for statistical analysis. Significance was designated at $p < 0.05$.

Results

Islet Function

In vitro function of isolated islets demonstrated excellent viability (91.4 ± 3.4 %: n = 5 isolations) with a mean SI of 11.4 ± 0.3 and mean insulin content of 26.3 ± 0.4 ng/islet.

DCE MRI Findings

A sample time sequence of images from a typical DCE scan illustrates the right (transplanted) and left (control) liver lobes (Fig. 4.1). Peak enhancement in the liver was seen 4 min after contrast injection, with a slow washout of contrast agent where all tissues showed some residual enhancement at the end of the 30-min scan. The time to peak enhancement was significantly earlier in the HBO group, especially at POD 14 (HBO vs. Control: 4.7 ± 0.2 vs. 5.2 ± 0.2 min at POD 3 ($p = 0.07$), 4.8 ± 0.3 vs. 5.4 ± 0.7 min at POD 7 ($p = 0.22$), 4.5 ± 0.1 vs. 5.5 ± 0.2 min at POD 14 ($p = 0.002$)). Normalized temporal enhancement curves between the HBO and control groups at POD 3, 7, and 14 revealed no significant differences between the experimental groups at POD 3 and 14 (Fig. 4.2A, C). However at POD 7, the DCE in the HBO animals was reduced compared to the control group (Fig. 4.2B). The DCE ratio at POD 7 compared to POD 3 was significantly ($p = 0.03$) decreased in the HBO group (Fig. 4.2D) consistent with decreased leakage of the contrast agent at POD 7.

Evaluation of Vessels

Some islets associated with vWF-positive staining were found to occlude the portal vein (Fig. 4.3A) but very few newly formed vessels (vWF positive) around islets were observed at POD 3. The number of vWF stained cells adjacent to islets increased significantly at POD 7 and 14 (Fig. 4.3B, C).

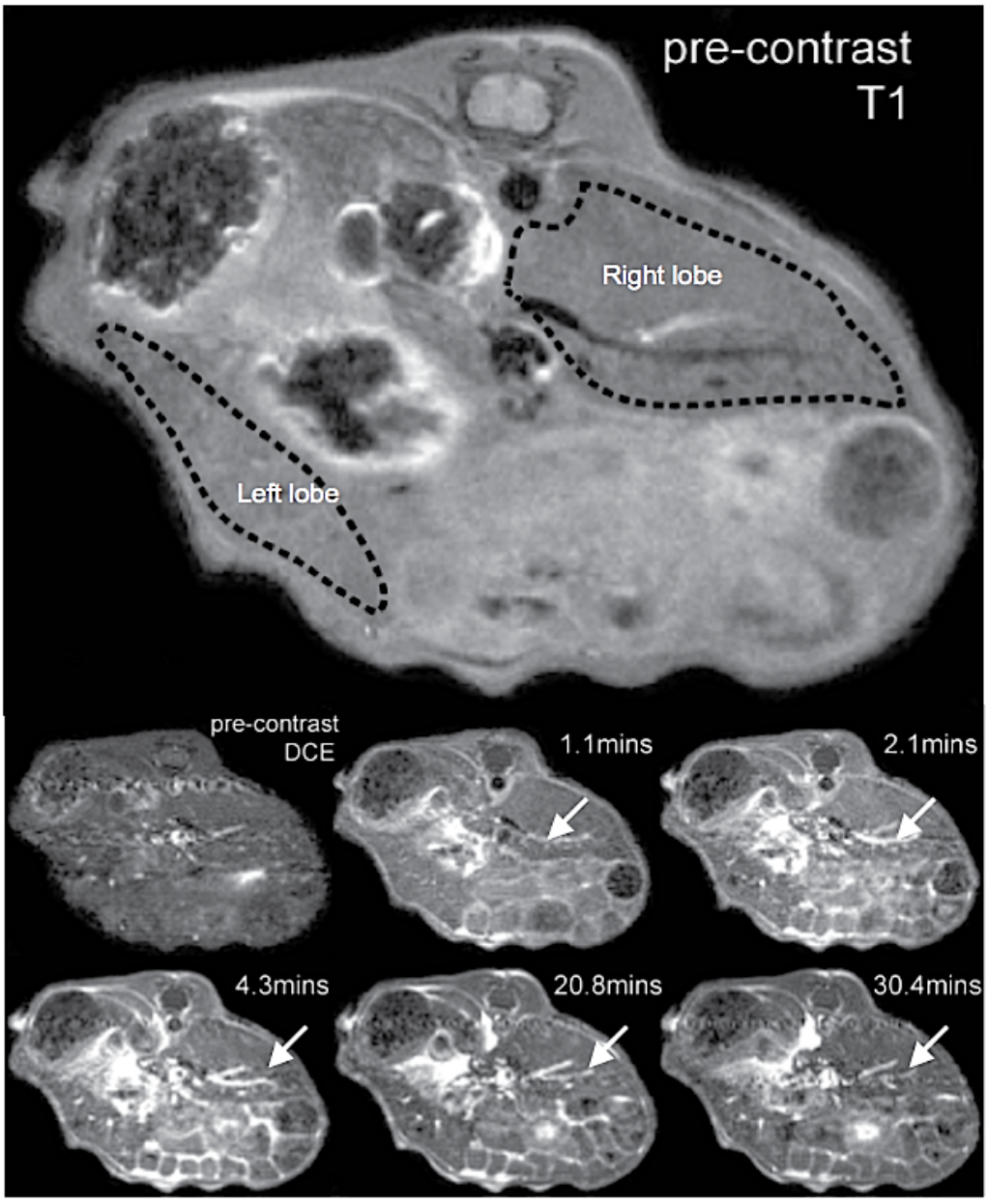

Figure 4.1. Dynamic contrast-enhanced magnetic resonance imaging (DCE MRI) enhancement after intraportal liver islet transplantation. Liver DCE MRI in an islet transplanted mouse at POD 7 after HBO therapy demonstrates enhancement after gadolinium (Gd) injection. Liver images prior (0 min) and after (1, 2, 4, 20, and 30 min) Gd injection demonstrated peak enhancement at 4 min. The increased concentration of contrast agent in the intravascular space can be visualized by enhancement of the portal vein (arrows).

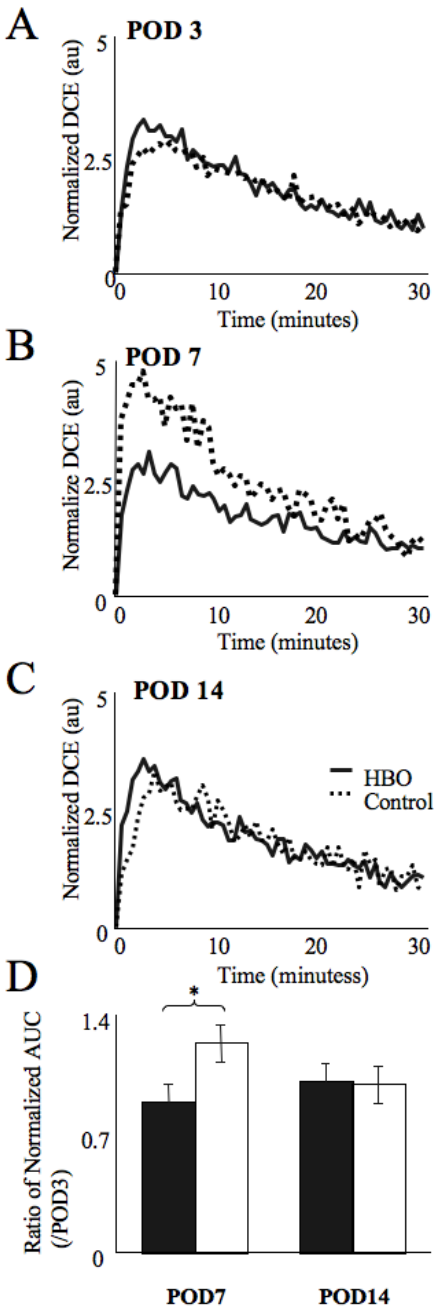

Figure 4.2. Quantification of dynamic contrast-enhanced magnetic resonance imaging. (A–C) Normalized DCE enhancement curves at POD 3 (A), 7 (B), and 14 (C). HBO inhibited the increase in contrast enhancement found in controls (no HBO) at POD 7. (D) The DCE ratio at POD 7 or 14 compared to POD 3 revealed a significant decrease in enhancement at POD 7 after HBO therapy. *$p < 0.05$.

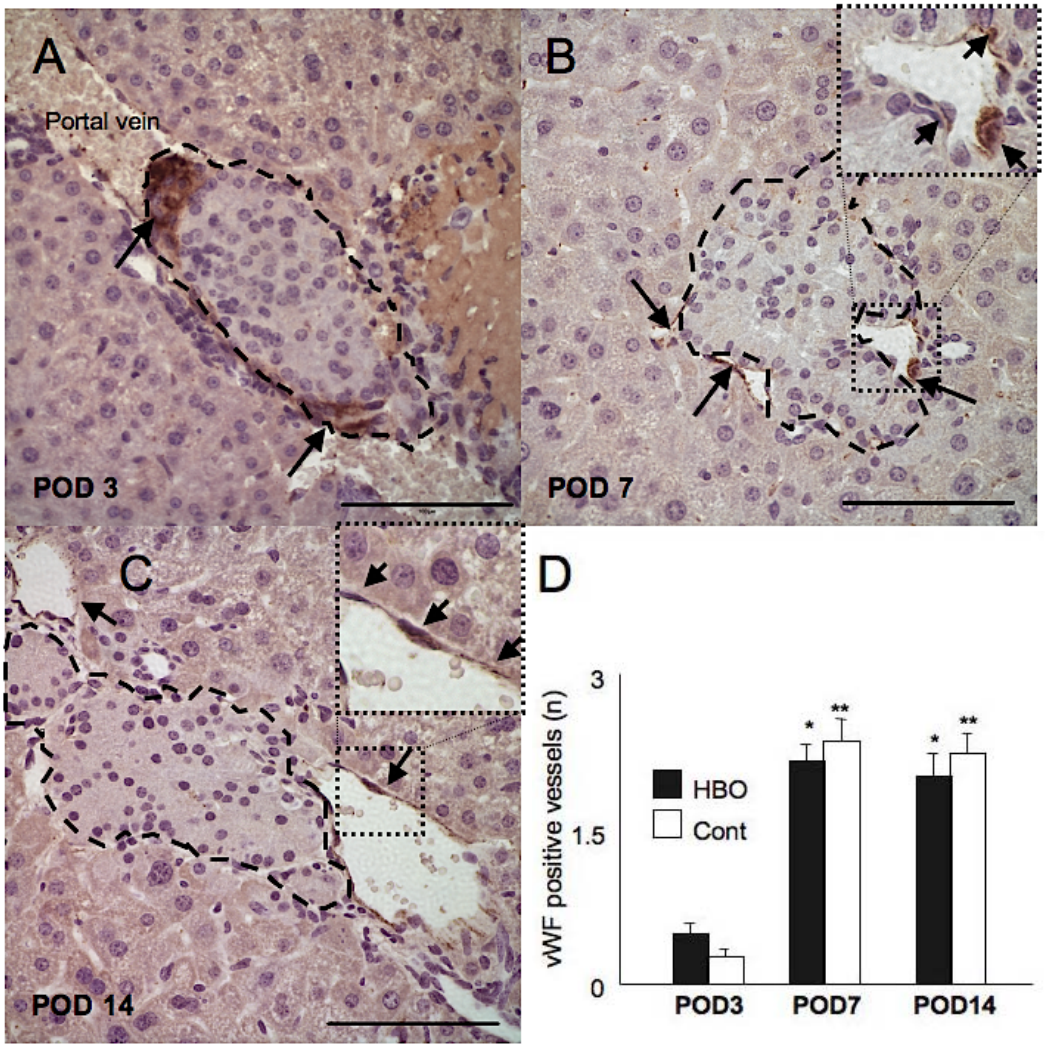

Figure 4.3. Islets stained with von Willebrand Factor (vWF) for new vessel formation. At POD 3 islets (dotted line) were stained with vWF (indicated as arrow) but there were few newly formed vessels (A). At POD 3 vWF stained areas were considered as coagula. Vessel formation around islets (arrows) were more prominent at POD 7 (B) and 14 (C) (see expanded insets). Figures are from control mice. (D) Quantified vWF staining was significantly increased at POD 7 and 14 compared to POD 3 in both groups (*$p < 0.0001$ in HBO group and **$p < 0.0001$ in control group, Dunnet test). Calibration bars = 100 μm.

The average number of new vessels seen associated with islets were 0.5 ± 0.1 in the HBO and 0.2 ± 0.1 in the control group at POD 3 (Fig. 4.3D) which was significantly increased in both groups at POD 7 and 14 ($p < 0.0001$, Fig. 4.3B–D). There were no significant differences in the number of newly formed vessels between the HBO and control groups at any time point.

Histological Findings on Islets and Liver Tissue

Transplanted islets and surrounding liver tissue showed signs of severe hypoxia (HIF-1α positive), apoptosis (TUNEL positive) and necrosis at POD 3 that was significantly decreased by POD 7 in both groups (Fig. 4.4). POD 14 showed a return to normoxia in islets and liver tissue with no apoptosis or necrosis (Fig. 4.4). VEGF was also expressed prominently at POD 3 but was reduced at POD 7 and 14 (Fig. 4.4).

At POD 3, the percentage of islet cells that stained positive for HIF-1α was 42.6 ± 6.1% in HBO (n = 67 islets from two mice) and 53.2 ± 7.1% in control groups (n = 50 islets from two mice). There was a significant decrement in islet hypoxia after HBO compared to the non-HBO control group at POD 7 (0.4 ± 0.2 vs. 2.1 ± 0.7%: $p = 0.02$, Figs 4.4 and 4.5A). There were also fewer apoptotic islet cells at POD 3 in the HBO group (43.3 ± 6.3%, n = 67 islets) compared to the control group (51.5 ± 7.0%, n = 50 islets). The number of apoptotic islet cells was significantly lower at POD 7 in the HBO group (1.7 ± 0.7%, n = 51 islets) compared to 5.7 ± 1.5% in the control group (n = 56 islets) ($p = 0.01$) (Figs 4.4 and 4.5B). VEGF was also prominently diminished in HBO group compared with the non-HBO group at POD 7 (0.01 ± 0.01 vs. 4.7 ± 1.9%: p =

0.01, Fig. 4.5C). Necrotic islets were observed at POD 3 but not at POD 7 and 14 (data not shown) but there was no significant difference between groups.

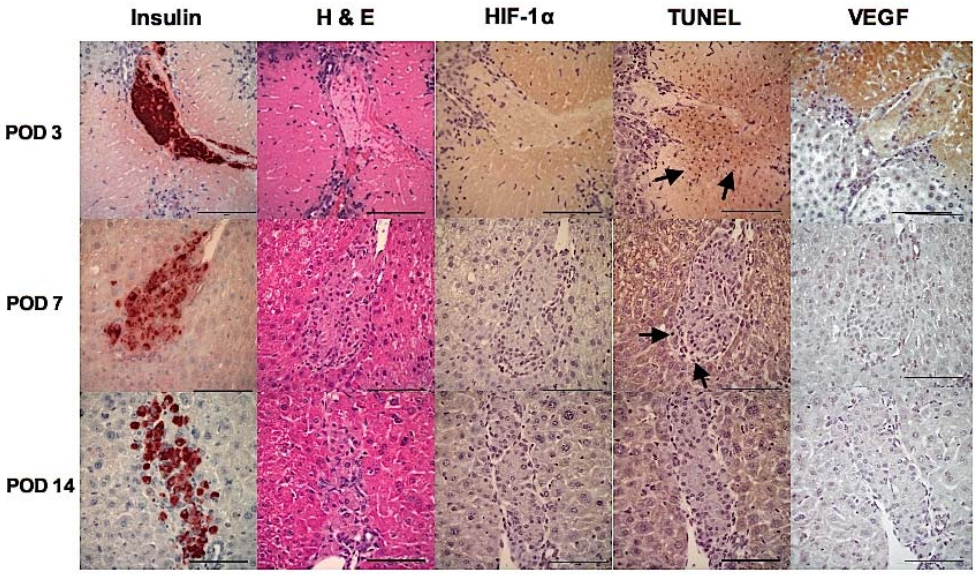

Figure 4.4. Histological findings at POD 3, 7, and 14. Insulin staining revealed the location of the islets in liver tissues. Necrosis (H & E), hypoxia (HIF-1α) and apoptosis (TUNEL) of the islets and surrounding liver tissues were prominent at POD 3 but decreased after POD 7. Vascular endothelial growth factor (VEGF) was also prominent at POD 3 and decrement at POD7 and 14. Figures are from control mice. Arrows indicate apoptotic cells. Calibration bar = 100 μm.

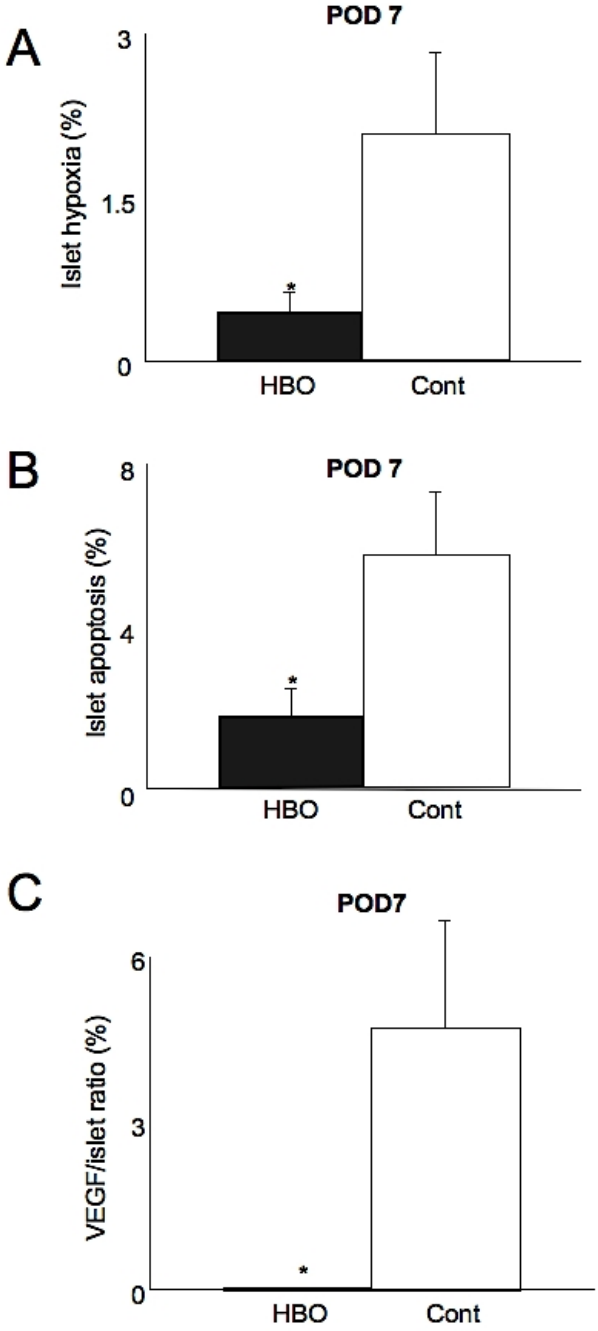

Figure 4.5. Quantification of histological assessment at POD 7. (A) Hypoxic islet cells (HIF-1α positive staining) were significantly decreased in animals undergoing HBO therapy. (*p = 0.02). (B) Apoptotic islet cells (TUNEL positive) were also significantly decreased after transplantation of islets in mice that underwent HBO therapy. (*p = 0.01). (C) Vascular endothelial growth factor (VEGF) positive islet cells were prominently decreased in HBO group at POD 7 (*p = 0.01). Decreased HIF-1α may contribute to a decrease in VEGF expression.

Liver hypoxia assessed by HIF-1α staining was transiently elevated at POD 3 and was zero at POD 7 and 14 in both groups ($p < 0.0001$). A similar pattern was observed for necrosis (H & E) where the HBO group had some TUNEL positive staining at POD 3 that disappeared at POD 7 and 14, with no significant difference between HBO and control groups (data not shown). The proportion of apoptotic liver tissue in both groups was over 60% at POD 3 and returned to zero by POD7 ($p < 0.0001$).

In summary, over half of the total islets and the surrounding liver tissue were apoptotic and necrotic at POD 3 but both dramatically decreased by POD 7 in the HBO-treated animals compared to non-HBO controls. There was a significant improvement in HBO group at POD 7 in islet hypoxia and apoptosis and a related decrement in VEGF expression in the HBO group at POD 7.

Blood Glucose, Serum Insulin, and GTT

The serum insulin and GTT data were acquired from all mice included in this study. Serum insulin levels were significantly higher (Fig. 4.6A; $p = 0.04$) and GTT was significantly lower in HBO-treated mice at POD 7 (Fig. 4.6B; $p = 0.04$) after HBO treatment compared to controls. However, there were no significant differences in serum insulin and GTT at POD 14 (data not shown), and no significant differences in blood glucose levels between the two groups. Normoglycemia was achieved in 44.4% (4/9 mice) of the HBO and 30% (3/10 mice) of the control group. Days to normoglycemia took an average of 5.3 ± 1.8 d in the HBO group and 6.3 ± 5.3 d in the control group ($p = 0.77$).

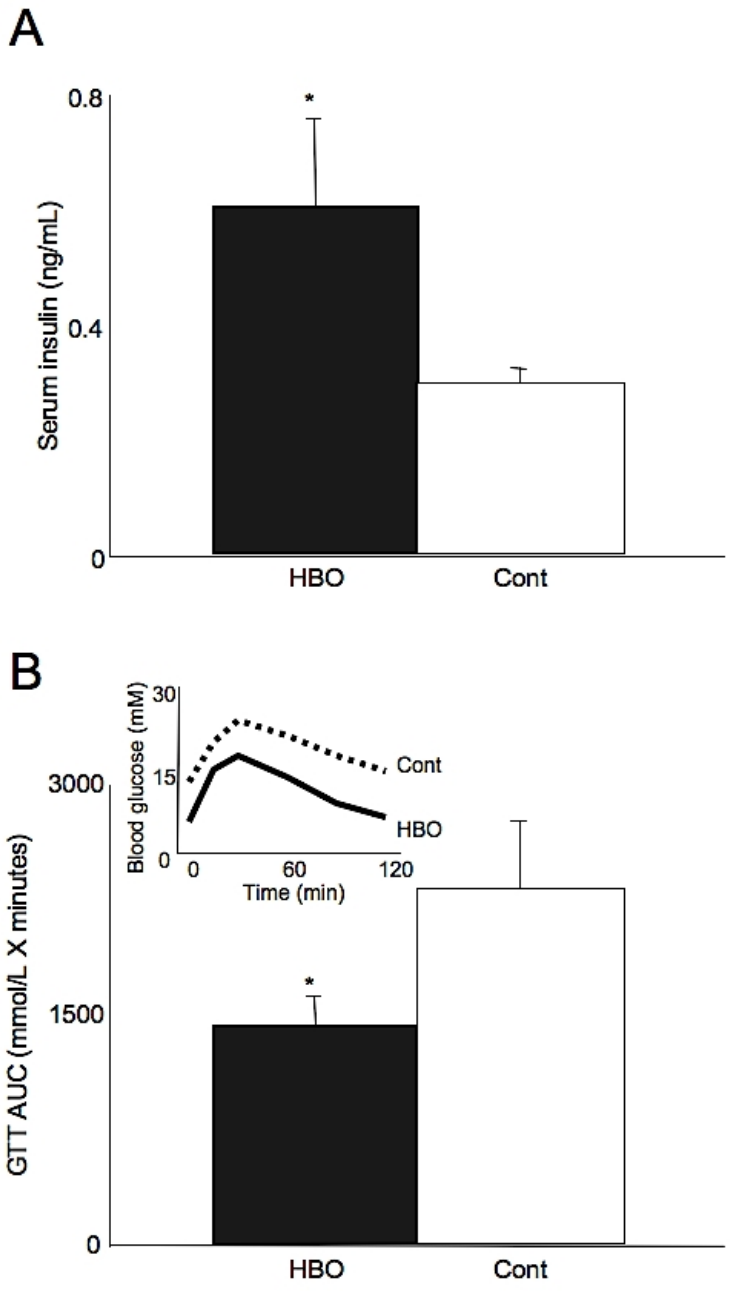

Figure 4.6. HBO improves functional outcomes after intraportal islet transplant. (A) A significant increase in serum insulin levels was observed in HBO-treated animals at POD7. (*p = 0.04). (B) Glucose tolerance test (GTT) was also significantly improved after HBO therapy at POD 7. (*p = 0.04). The GTT insert illustrates a typical time course response.

Discussion

HBO is a therapeutic option for clinical and experimental conditions associated with increased or acute hypoxia. The mechanisms underlying the therapeutic effectiveness of HBO appear to be related to a reduction in tissue hypoxia, decreased levels of cytokines (TNF-α or IL-1), reduction in the affinity of major histocompatibility complex (MHC) class I specific antibodies, and inhibition of apoptosis (22).

This study on the therapeutic effectiveness of HBO after islet transplants in diabetic mice found: (i) a significant decrease in contrast enhancement within the liver of the HBO group, (ii) a significant decrease in islet hypoxia and apoptosis after HBO therapy compared to controls, (iii) a significant decrease in VEGF expression at POD 7, (iv) that serum insulin production was twofold higher in HBO-treated mice at POD 7, and 5) improved glucose tolerance in HBO-treated mice at POD 7. A significant increase in neovascularization was seen in both HBO and non-HBO groups at POD 7 and 14, despite lack of significant difference between the two groups. In this study, HBO therapy decreased hypoxia and apoptosis and ultimately lead to improved islet function. There was no significant difference in histologically detected neovascularization between the HBO and control groups. Our lab has previously shown the beneficial effects of HBO treatment on subcapsular islet grafts (14), but knowledge of the HBO effect on intraportal islets as described by the authors of this study is new.

The study evaluated the therapeutic potential of HBO treatment after intraportal islet transplantation on neovascularization. We (8, 9) have previously shown that DCE MRI can provide an indirect measure of neovascularization in a variety of animal models. DCE MRI showed peak enhancement at POD7 in control animals, consistent with islet

angiogenesis (10, 23). However, this increased angiogenesis was not observed after HBO therapy at POD 7. Our histological data showed decreased HIF-1α and VEGF staining in the HBO group and no differences between HBO and control groups in the number of peri-islet vWF-positive vessels. These findings would suggest that HBO therapy results in a less permeable peri-islet neovasculature at POD 7 with no net change in the number of new vessels. More importantly, earlier new vessel maturation would result in decreased hypoxia and improved functional outcomes after islet transplant in diabetic mice (see below).

One possible explanation is that a permeable neovasculature is a result of increased VEGF, in part because of upregulation of HIF-1α, as seen in our control animals (24–26). It is well known that HIF-1α upregulates VEGF under ischemic conditions and VEGF contributes to a leaky and destabilized vasculature (27, 28). However, previous reports have shown that HBO reduces VEGF production in a mouse ischemic hind limb model (29). Thus a potential mechanism underlying our results is that HBO-related HIF-1α reduction is followed by a strong reduction in VEGF expression. This cascade then leads to decreased permeability in newly formed vessels adjacent to transplanted islets which results in reduced enhancement of DCE at POD 7. In support of this proposed mechanism is a recent report which demonstrated that increased VEGF production delays vessel maturation (27). Thus, our data would suggest that decrements in hypoxia and subsequent decreases inVEGFaccelerate the development of mature vessels, which then results in decreased contrast extravasation (DCE MRI).

HBO therapy led to a significant decrease in islet hypoxia and apoptosis at POD 7 that lead to a significant increase in serum insulin production and improved glucose

tolerance. Thus, HBO effectively rescued a subset of transplanted islets from hypoxic injury and apoptosis and as a consequence improved their function. We noted that the effects of HBO therapy on intraportal islets in our current study did not appear to be as robust as those previously reported after renal subcapsular transplants (14). These differences could be related to the vascular (intraportal) route which is known to elicit an instant blood-mediated inflammatory reaction (IBMIR) (30). IBMIR is characterized by activation of platelets and complement when islets are exposed to fresh blood (30). Islet damage related to IBMIR can be detected within an hour (31), thus potentially leading to significant islet damage prior to or during the HBO procedure. Therefore, HBO effectiveness in protecting transplanted islets could be enhanced by the simultaneous treatment of IBMIR. Furthermore, recent reports suggest that embolization of the portal vein by the islets themselves could be a major cause of early islet graft loss (4, 18). In our experience (32), we detected near total obstruction of the portal vein with 90% of the surrounding liver tissue exhibiting hypoxia/apoptosis at early posttransplant time points. Islet damage caused by embolization is presumably related to local liver tissue ischemia (4). This local ischemia is also likely reduced in HBO-treated animals providing a healthy environment for the transplanted islets to generate new vasculature to support their survival and function. To reduce the influence of embolization, smaller islets and a larger animal model could also be used thereby improving the efficacy of HBO therapy. Moreover, longer courses of HBO treatment (for example, 7–14 d) might be more effective in promoting islet function. HBO therapy prior to transplantation should also be considered as this may induce endothelial progenitor stem cell differentiation into vascular endothelial cells, further preventing ischemia and improving glycemic control.

Actually, some studies revealed that HBO stimulates endothelial progenitor stem cells in animal models of ischemia (25, 33).

In conclusion, our data support the potential effectiveness of HBO treatment following intraportal islet transplantation in maintaining a more receptive healthy liver environment and improving islet function. There is a possibility that intensive more prolonged HBO would further improve therapeutic outcome. Non-invasive imaging, such as DCE MRI can monitor neovascularization and may indicate enhanced vascular maturation after therapeutic interventions.

Acknowledgements

This work was supported by NIH/NIDDK Grant # 1R01-DK077541 (E. H.), a grant from the National Medical Test Bed (E. H.) and a research fellowship from the Uehara Memorial Foundation (N. S.). We are very appreciative of the microsurgical technical support of the Loma Linda University Microsurgery Laboratory and the kind help in specimen processing by John Hough.

References

1. International Islet Transplant Registry. Newsletter. 2001: 9.

2. Ryan EA, Paty BW, Senior PA et al. Five-year followup after clinical islet transplantation. Diabetes 2005: 54: 2060–2069.

3. Shapiro AM, Lakey JR, Ryan EA et al. Islet transplantation in seven patients with type 1 diabetesmellitus using a glucocorticoid-free immunosuppressive regimen. N Engl J Med 2000: 343: 230–238.

4. Yin D, Ding JW, Shen J, Ma L, Hara M, Chong AS. Liver ischemia contributes to early islet failure following intraportal transplantation: benefits of liver ischemicpreconditioning. Am J Transplant 2006: 6: 60–68.

5. Biarnes M, Montolio M, Nacher V, Raurell M, Soler J, Montanya E. Beta-cell death and mass in syngeneically transplanted islets exposed to short- and long-term hyperglycemia. Diabetes 2002: 51: 66–72.

6. Evgenov NV, Medarova Z, Dai G, Bonner-Weir S, Moore A. In vivo imaging of islet transplantation. Nat Med 2006: 12: 144–148.

7. Jirak D, Kriz J, Herynek V et al. MRI of transplanted pancreatic islets. Magn Reson Med 2004: 52: 1228–1233.

8. Hathout E, Sowers L, Wang R et al. In vivo magnetic resonance imaging of vascularization in islet transplantation. Transpl Int 2007: 20: 1059–1065.

9. Hathout E, Chan NK, Tan A et al. In vivo imaging demonstrates a time-line for new vessel formation in islet transplantation. Pediatr Transplant 2009: 13: 892–897.

10. Chan NK, Obenaus A, Tan A et al. Monitoring neovascularization of intraportal islet grafts by dynamic contrast enhanced magnetic resonance imaging. Islets 2009: 1. [Epub ahead of print].

11. Moritz W, Meier F, Stroka DM et al. Apoptosis in hypoxic human pancreatic islets correlates with HIF- 1alpha expression. FASEB J 2002: 16: 745–747.

12. Lepore DA, Shinkel TA, Fisicaro N et al. Enhanced expression of glutathione peroxidase protects islet beta cells from hypoxia-reoxygenation. Xenotransplantation 2004: 11: 53–59.

13. Jones GL, Juszczak MT, Hughes SJ, Kooner P, Powis SH, Press M. Time course and quantification of pancreatic islet revascularization following intraportal transplantation. Cell Transplant 2007: 16: 505–516.

14. Miao G, Ostrowski RP, Mace J et al. Dynamic production of hypoxia-inducible factor-1alpha in early transplanted islets. Am J Transplant 2006: 6: 2636–2643.

15. Gotoh M, Maki T, Kiyoizumi T, Satomi S, Monaco AP. An improved method for isolation of mouse pancreatic islets. Transplantation 1985: 40: 437–438.

16. Sakata N, Egawa S, Sumi S, Unno M. Optimization of glucose level to determine the stimulation index of isolated rat islets. Pancreas 2008: 36: 417–423.

17. Yonekawa Y, Okitsu T, Wake K et al. A new mouse model for intraportal islet transplantation with limited hepatic lobe as a graft site. Transplantation 2006: 82: 712–715.

18. Sakata N, Hayes P, Tan A et al. MRI assessment of ischemic liver after intraportal islet transplantation. Transplantation 2009: 87: 825–830.

19. Sakata N, Tan A, Chan N et al. Efficacy comparison between intraportal and subcapsular islet transplants in a murine diabetic model. Transplant Proc 2009: 41: 346–349.

20. Forleo C, Resta N, Sorrentino S et al. Association of beta-adrenergic receptor polymorphisms and progression to heart failure in patients with idiopathic dilated cardiomyopathy.AmJMed 2004: 117: 451–458.

21. Tofts PS. Modeling tracer kinetics in dynamic Gd- DTPA MR imaging. J Magn Reson Imaging 1997: 7: 91–101.

22. Muralidharan V, Christophi C. Hyperbaric oxygen therapy and liver transplantation. HPB (Oxford) 2007: 9: 174–182.

23. Menger MD, Jaeger S, Walter P, Feifel G, Hammersen F, Messmer K. Angiogenesis and hemodynamics of microvasculature of transplanted islets of Langerhans. Diabetes 1989: 38 (Suppl. 1): 199–201.

24. Sepulveda P,Martinez-Leon J, Garcia-Verdugo JM. Neoangiogenesis with endothelial precursors for the treatment of ischemia. Transplant Proc 2007: 39: 2089–2094.

25. Milovanova TN, Bhopale VM, Sorokina EM et al. Hyperbaric oxygen stimulates vasculogenic stem cell growth and differentiation in vivo. J Appl Physiol 2009: 106: 711–28.

26. Dai Y, Xu M, Wang Y, Pasha Z, Li T, Ashraf M. HIF-1alpha induced-VEGF overexpression in bone marrow stem cells protects cardiomyocytes against ischemia. J Mol Cell Cardiol 2007: 42: 1036–1044.

27. Greenberg JI, Shields DJ, Barillas SG et al. A role for VEGF as a negative regulator of pericyte function and vessel maturation. Nature 2008: 456: 809–813.

28. Ozawa CR, Banfi A, Glazer NL et al.Microenvironmental VEGF concentration, not total dose, determines a threshold between normal and aberrant angiogenesis. J Clin Invest 2004: 113: 516–527.

29. Asano T, Kaneko E, Shinozaki S et al. Hyperbaric oxygen induces basic fibroblast growth factor and hepatocyte growth factor expression, and enhances blood perfusion and muscle regeneration in mouse ischemic hind limbs. Circ J 2007: 71: 405–411.

30. Bennet W, Groth CG, Larsson R, Nilsson B, Korsgren O. Isolated human islets trigger an instant blood mediated inflammatory reaction: implications for intraportal islet transplantation as a treatment for patients with type 1 diabetes. Ups J Med Sci 2000: 105: 125–133.

31. Johansson H, Lukinius A, Moberg L et al. Tissue factor produced by the endocrine cells of the islets of Langerhans is associated with a negative outcome of clinical islet transplantation. Diabetes 2005: 54: 1755–1762.

32. Sakata N, Obenaus A, Chan N, Mace J, Chinnock R, Hathout E. Factors affecting islet graft embolization in the liver of diabetic mice. Islets 2009: 1: 26–33.

33. Goldstein LJ, Gallagher KA, Bauer SM et al. Endothelial progenitor cell release into circulation is triggered by hyperoxia-induced increases in bone marrow nitric oxide. Stem Cells 2006: 24: 2309–2318.

CHAPTER FIVE

DISCUSSION

In this series of studies, we were able to successfully meet our three specific aims with DCE MRI. Specifically, DCE MRI non-invasively established a time course of islet angiogenesis in subcapsular and intraportal islet grafts consistent with previous reports, and assessed the effect of a pro-angiogenic hyperbaric oxygen therapy. While these results are promising, there are limitations in the current imaging protocol that will need to be addressed before moving forward to pre-clinical large animal and clinical human trials.

Limitations

One limitation of the current DCE MRI protocol is that it is less sensitive to intraportal islet angiogenesis (Fig. 3.2) than subcapsular islet angiogenesis (Fig. 2.3). This is related in part to the dispersed nature of the intraportal islets, and the well perfused nature of the background liver parenchyma. The conventional two-compartment Tofts model used for DCE MRI analysis (Tofts 1991) takes into account permeability between only the intravascular and extracellular spaces. This model is suitable for analysis of large aggregates of cells such as tumors and subcapsular islet grafts, but may be suboptimal for intraportal grafts as the unique hepatic vasculature is comprised of both arterial and portal blood supplies. DCE MRI analysis of intraportal islet grafts using a dual-input one compartment model (Materne 2002, Baxter 2009) may

yield more reliable estimates of vascular permeability and thus vessel maturity. Another liver-specific dual input five compartment DCE MRI has also been more recently described (Mescam 2009). Another limitation of the Tofts model is that it may over- or under-estimate absolute capillary permeability depending on capillary diameter (Correia Carreira 2011). For our purposes however, accurate absolute quantification is less of a concern than tracking relative changes in permeability over time.

All DCE MRI models require an arterial input function (AIF) that is the time course of contrast concentration in the intravascular space. These values can be hard to measure accurately, especially when imaging the liver, which is susceptible to respiratory motion artifacts. Additionally, there is an inherent tradeoff between minimizing partial volume effects of the aorta region of interest by increasing spatial resolution but at the expense of decreasing temporal resolution and potentially missing the peak of contrast enhancement. One way to address this issue is to calculate an AIF based on the enhancement of a known and well-characterized reference tissue. By assigning literature values for various properties of the reference tissue, a presumptive AIF can be calculated without having to measure it directly (Yankeelov 2005, Yankeelov 2006, Yankeelov 2007, Yankeelov 2008). Reference region modeling is also robust against poor temporal sampling resolution (Planey 2009). Muscle is a good candidate reference tissue in future animal and human studies.

It is important to note that the use of gadolinium based contrast agents is generally well tolerated and safe, but administration in individuals with kidney failure can result in nephrogenic systemic fibrosis (NSF), which involves fibrosis of the skin, joints, eyes, and in severe cases, internal organs. As diabetic nephropathy is a common complication of

diabetes, confirming adequate renal function (glomerular filtration rate >60 ml/min) (Kanal 2007) before imaging will be necessary.

Future Directions

In addition to hyperbaric oxygen therapy, there are other pro-angiogenic strategies that are under active investigation. One exciting avenue is the use of co-transplanted cells to stimulate angiogenesis. Our laboratory was the first to co-transplant bone marrow cells with islets (Sakata 2010). Preliminary images from those animals were unable to undergo DCE MRI analysis due to the confounding effect of negative contrast from the large number of bone marrow cells that were Feridex-labeled for histological assessment (unpublished data). Subsequent studies by others have shown that mesenchymal stem cells (MSC) are the specific bone marrow-derived cell population responsible for the pro-angiogenic effect (Ito 2010). MSC co-transplantation may be made even more effective by creating composite stem cell coated islets (Duprez 2011) that are particularly well suited to intraportal transplantation. Since our intraportal DCE MRI protocol does not depend on islet labeling, we expect it to be sensitive to the potential angiogenic differences between such MSC coated and uncoated islets. Bioengineering approaches to shield cell surfaces from immune recognition (Nilsson 2010) and cell surface modification with growth factors (Cabric 2010) are other promising pro-angiogenic strategies that are equally amenable to non-invasive imaging.

More effective sites of transplantation are also being sought. Transplantation into muscle has been shown in animal models (Christoffersson 2010) as well as humans (Rafael 2008). Since intramuscular islets are closer to the surface of the body, they may

be very good candidates for contrast imaging, which can be done with high sensitivity surface coils. If the islets are in the muscles of the arms or legs, there is even the possibility of making perfusion measurements by arterial spin labeling, which would obviate the need for exogenous contrast administration. Other transplantation sites include some that offer potentially good MR signal such as the submandibular gland (Sandberg 2011) and small intestine (Kakabadze 2011) and some sites that have less signal such as bone marrow (Salazar-Banuelos 2008).

The progress made in just the last decade of islet transplantation has been encouraging, but they have also exposed all the challenges that remain, and highlight the need for further research into realizing the promise of one day finding a cure for type 1 diabetes.

REFERENCES

1. Banting FG, Best CH, Collip JB, Campbell WR, Fletcher AA. Pancreatic Extracts in the Treatment of Diabetes Mellitus. *Can Med Assoc J*. 1922;12:141-146

2. Aanstoot HJ, Anderson BJ, Daneman D, Danne T, Donaghue K, Kaufman F, Rea RR, Uchigata Y. The global burden of youth diabetes: perspectives and potential. *Pediatr Diabetes*. 2007;8 Suppl 8:1-44

3. Atkinson MA, Bluestone JA, Eisenbarth GS, Hebrok M, Herold KC, Accili D, Pietropaolo M, Arvan PR, Von Herrath M, Markel DS, Rhodes CJ. How Does Type 1 Diabetes Develop?: The Notion of Homicide or {beta}-Cell Suicide Revisited. *Diabetes*. 2011;60:1370-1379

4. Redondo MJ, Fain PR, Eisenbarth GS. Genetics of type 1A diabetes. *Recent Prog Horm Res*. 2001;56:69-89

5. Kaprio J, Tuomilehto J, Koskenvuo M, Romanov K, Reunanen A, Eriksson J, Stengard J, Kesaniemi YA. Concordance for type 1 (insulin-dependent) and type 2 (non-insulin-dependent) diabetes mellitus in a population-based cohort of twins in Finland. *Diabetologia*. 1992;35:1060-1067

6. Knip M, Veijola R, Virtanen SM, Hyoty H, Vaarala O, Akerblom HK. Environmental triggers and determinants of type 1 diabetes. *Diabetes*. 2005;54 Suppl 2:S125-136

7. Bour-Jordan H, Bluestone JA. Regulating the regulators: costimulatory signals control the homeostasis and function of regulatory T cells. *Immunol Rev*. 2009;229:41-66

8. McClymont SA, Putnam AL, Lee MR, Esensten JH, Liu W, Hulme MA, Hoffmuller U, Baron U, Olek S, Bluestone JA, Brusko TM. Plasticity of human regulatory T cells in healthy subjects and patients with type 1 diabetes. *J Immunol*. 2011;186:3918-3926

9. Bluestone JA, Herold K, Eisenbarth G. Genetics, pathogenesis and clinical interventions in type 1 diabetes. *Nature*. 2010;464:1293-1300

10. Turka LA, Wood K, Bluestone JA. Bringing transplantation tolerance into the clinic: lessons from the ITN and RISET for the Establishment of Tolerance consortia. *Curr Opin Organ Transplant*. 2010;15:441-448

11. Ishiyama K, Rawson J, Omori K, Mullen Y. Liver natural killer cells play a role in the destruction of islets after intraportal transplantation. *Transplantation*. 2011;91:952-960

12. Scharp DW, Lacy PE, Santiago JV, McCullough CS, Weide LG, Falqui L, Marchetti P, Gingerich RL, Jaffe AS, Cryer PE, et al. Insulin independence after islet transplantation into type I diabetic patient. *Diabetes*. 1990;39:515-518

13. Ricordi C, Socci C, Davalli AM, Staudacher C, Vertova A, Baro P, Sassi I, Braghi S, Guizzi N, Pozza G, et al. Application of the automated method to islet isolation in swine. *Transplant Proc*. 1990;22:784-785

14. Tzakis AG, Ricordi C, Alejandro R, Zeng Y, Fung JJ, Todo S, Demetris AJ, Mintz DH, Starzl TE. Pancreatic islet transplantation after upper abdominal exenteration and liver replacement. *Lancet*. 1990;336:402-405

15. Shapiro AM, Lakey JR, Ryan EA, Korbutt GS, Toth E, Warnock GL, Kneteman NM, Rajotte RV. Islet transplantation in seven patients with type 1 diabetes mellitus using a glucocorticoid-free immunosuppressive regimen. *N Engl J Med*. 2000;343:230-238

16. Ryan EA, Paty BW, Senior PA, Bigam D, Alfadhli E, Kneteman NM, Lakey JR, Shapiro AM. Five-year follow-up after clinical islet transplantation. *Diabetes*. 2005;54:2060-2069

17. Nyman LR, Wells KS, Head WS, McCaughey M, Ford E, Brissova M, Piston DW, Powers AC. Real-time, multidimensional in vivo imaging used to investigate blood flow in mouse pancreatic islets. *J Clin Invest*. 2008;118:3790-3797

18. Miao G, Ostrowski RP, Mace J, Hough J, Hopper A, Peverini R, Chinnock R, Zhang J, Hathout E. Dynamic production of hypoxia-inducible factor-1alpha in early transplanted islets. *Am J Transplant*. 2006;6:2636-2643

19. Knopp MV, Giesel FL, Marcos H, von Tengg-Kobligk H, Choyke P. Dynamic contrast-enhanced magnetic resonance imaging in oncology. *Top Magn Reson Imaging*. 2001;12:301-308

20. Padhani AR, Husband JE. Dynamic contrast-enhanced MRI studies in oncology with an emphasis on quantification, validation and human studies. *Clin Radiol*. 2001;56:607-620

21. Yankeelov TE, Gore JC. Dynamic Contrast Enhanced Magnetic Resonance Imaging in Oncology: Theory, Data Acquisition, Analysis, and Examples. *Curr Med Imaging Rev*. 2009;3:91-107

22. Jordan BF, Runquist M, Raghunand N, Gillies RJ, Tate WR, Powis G, Baker AF. The thioredoxin-1 inhibitor 1-methylpropyl 2-imidazolyl disulfide (PX-12) decreases

vascular permeability in tumor xenografts monitored by dynamic contrast enhanced magnetic resonance imaging. *Clin Cancer Res*. 2005;11:529-536

23. Paldino MJ, Barboriak DP. Fundamentals of quantitative dynamic contrast-enhanced MR imaging. *Magn Reson Imaging Clin N Am*. 2009;17:277-289

24. Tofts PS, Kermode AG. Measurement of the blood-brain barrier permeability and leakage space using dynamic MR imaging. 1. Fundamental concepts. *Magn Reson Med*. 1991;17:357-367

25. Materne R, Smith AM, Peeters F, Dehoux JP, Keyeux A, Horsmans Y, Van Beers BE. Assessment of hepatic perfusion parameters with dynamic MRI. *Magn Reson Med*. 2002;47:135-142

26. Baxter S, Wang ZJ, Joe BN, Qayyum A, Taouli B, Yeh BM. Timing bolus dynamic contrast-enhanced (DCE) MRI assessment of hepatic perfusion: Initial experience. *J Magn Reson Imaging*. 2009;29:1317-1322

27. Mescam M, Kretowski M, Bezy-Wendling J. Multiscale Model of Liver DCE-MRI Towards a Better Understanding of Tumor Complexity. *IEEE Trans Med Imaging*. 2009

28. Correia Carreira G, Gemeinhardt O, Gorenflo R, Beyersdorff D, Franiel T, Plendl J, Ludemann L. Limitations of the permeability-limited compartment model in estimating vascular permeability and interstitial volume fraction in DCE-MRI. *Magn Reson Imaging*. 2011;29:639-649

29. Yankeelov TE, Luci JJ, Lepage M, Li R, Debusk L, Lin PC, Price RR, Gore JC. Quantitative pharmacokinetic analysis of DCE-MRI data without an arterial input function: a reference region model. *Magn Reson Imaging*. 2005;23:519-529

30. Yankeelov TE, DeBusk LM, Billheimer DD, Luci JJ, Lin PC, Price RR, Gore JC. Repeatability of a reference region model for analysis of murine DCE-MRI data at 7T. *J Magn Reson Imaging*. 2006;24:1140-1147

31. Yankeelov TE, Cron GO, Addison CL, Wallace JC, Wilkins RC, Pappas BA, Santyr GE, Gore JC. Comparison of a reference region model with direct measurement of an AIF in the analysis of DCE-MRI data. *Magn Reson Med*. 2007;57:353-361

32. Yankeelov TE, Luci JJ, DeBusk LM, Lin PC, Gore JC. Incorporating the effects of transcytolemmal water exchange in a reference region model for DCE-MRI analysis: theory, simulations, and experimental results. *Magn Reson Med*. 2008;59:326-335

33. Planey CR, Welch EB, Xu L, Chakravarthy AB, Gatenby JC, Freehardt D, Mayer I, Meszeoly I, Kelley M, Means-Powell J, Gore JC, Yankeelov TE. Temporal sampling requirements for reference region modeling of DCE-MRI data in human breast cancer. *J Magn Reson Imaging*. 2009;30:121-134

34. Kanal E, Barkovich AJ, Bell C, Borgstede JP, Bradley WG, Jr., Froelich JW, Gilk T, Gimbel JR, Gosbee J, Kuhni-Kaminski E, Lester JW, Jr., Nyenhuis J, Parag Y, Schaefer DJ, Sebek-Scoumis EA, Weinreb J, Zaremba LA, Wilcox P, Lucey L, Sass N. ACR guidance document for safe MR practices: 2007. *AJR Am J Roentgenol*. 2007;188:1447-1474

35. Sakata N, Chan NK, Chrisler J, Obenaus A, Hathout E. Bone marrow cell cotransplantation with islets improves their vascularization and function. *Transplantation*. 2010;89:686-693

36. Ito T, Itakura S, Todorov I, Rawson J, Asari S, Shintaku J, Nair I, Ferreri K, Kandeel F, Mullen Y. Mesenchymal stem cell and islet co-transplantation promotes graft revascularization and function. *Transplantation*. 2010;89:1438-1445

37. Duprez IR, Johansson U, Nilsson B, Korsgren O, Magnusson PU. Preparatory studies of composite mesenchymal stem cell islets for application in intraportal islet transplantation. *Ups J Med Sci*. 2011;116:8-17

38. Nilsson B, Korsgren O, Lambris JD, Ekdahl KN. Can cells and biomaterials in therapeutic medicine be shielded from innate immune recognition? *Trends Immunol*. 2010;31:32-38

39. Cabric S, Sanchez J, Johansson U, Larsson R, Nilsson B, Korsgren O, Magnusson PU. Anchoring of vascular endothelial growth factor to surface-immobilized heparin on pancreatic islets: implications for stimulating islet angiogenesis. *Tissue Eng Part A*. 2010;16:961-970

40. Christoffersson G, Henriksnas J, Johansson L, Rolny C, Ahlstrom H, Caballero-Corbalan J, Segersvard R, Permert J, Korsgren O, Carlsson PO, Phillipson M. Clinical and experimental pancreatic islet transplantation to striated muscle: establishment of a vascular system similar to that in native islets. *Diabetes*. 2010;59:2569-2578

41. Rafael E, Tibell A, Ryden M, Lundgren T, Savendahl L, Borgstrom B, Arnelo U, Isaksson B, Nilsson B, Korsgren O, Permert J. Intramuscular autotransplantation of pancreatic islets in a 7-year-old child: a 2-year follow-up. *Am J Transplant*. 2008;8:458-462

42. Sandberg M, Carlsson F, Nilsson B, Korsgren O, Carlsson PO, Jansson L. Syngeneic islet transplantations into the submandibular gland of mice. *Transplantation*. 2011;91:e17-19

43. Kakabadze Z, Gupta S, Brandhorst D, Korsgren O, Berishvili E. Long-term engraftment and function of transplanted pancreatic islets in vascularized segments of small intestine. *Transpl Int*. 2011;24:175-183

44. Salazar-Banuelos A, Wright JR, Jr., Sigalet D, Benitez-Bribiesca L. Pancreatic islet transplantation into the bone marrow of the rat. *Am J Surg*. 2008;195:674-678; discussion 678

POSTSCRIPT

"Never let your schooling interfere with your education." -Mark Twain